National University of Singapore

Single-molecule studies of DNA organization by bacterial architectural proteins

LIN JIE – HT051204B

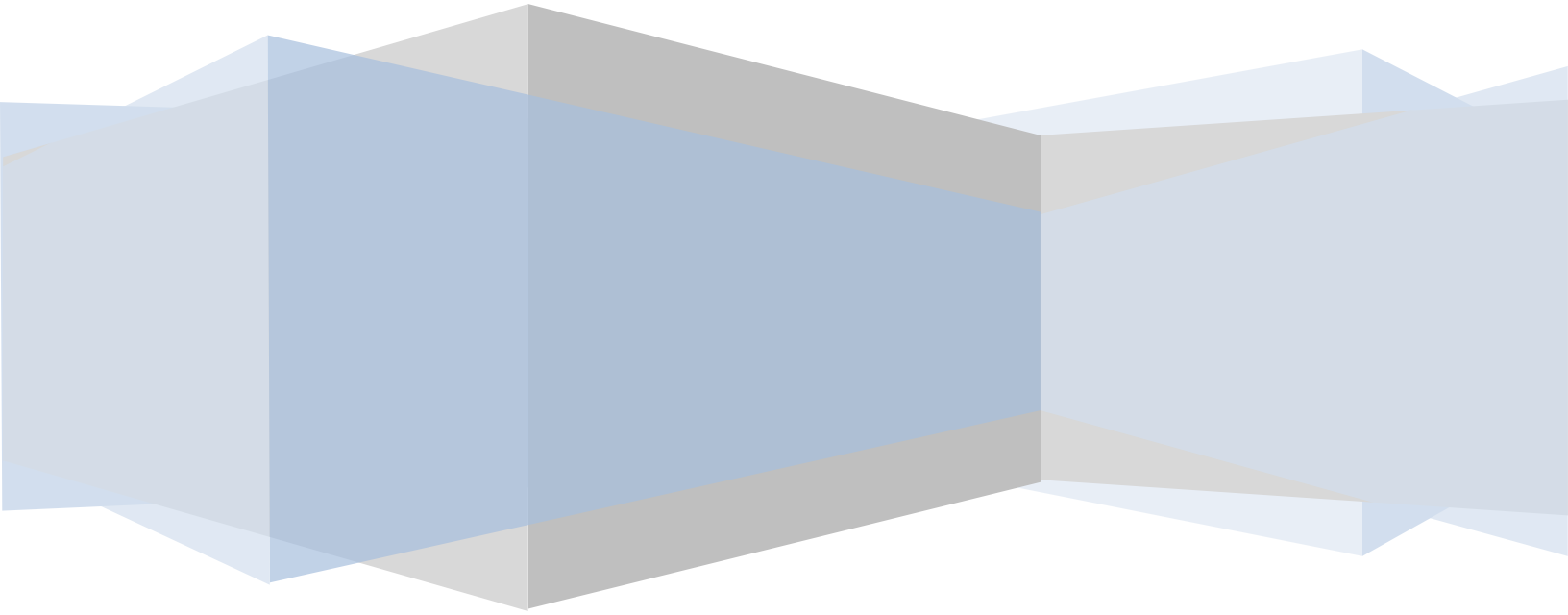

Acknowledgement

Special thank goes to Assoc Prof. YAN Jie, my PhD. supervisor, for his supervision and support. This thesis would not have been possible without his help.

I am also grateful to my collaborator Assoc Prof. Peter Droge for IHF protein expression and purification, Dr. CHEN Hu for the simulation, Assoc Prof. Linda J. Kenney for stimulating discussions, and all my lab mates for their help and suggestions.

Last but not the least I would like to thank my university, National University of Singapore, for offering me such a great opportunity to pursue my PhD. study.

Summary

In my PhD study, I focused on the project of non-specific DNA binding of IHF by using a combination of single DNA manipulation and atomic force microscopy imaging methods. The integration host factor (IHF) is an abundant nucleoid-associated protein and an essential co-factor for phage λ site-specific recombination and gene regulation in *E. coli*. Introduction of a sharp DNA kink at specific cognate sites is critical for these functions. Interestingly, the intra-cellular concentration of IHF is much higher than the concentration needed for site-specific interactions, suggesting that non-specific binding of IHF to DNA plays a role in the physical organization of bacterial chromatin. However, it is unclear how non-specific DNA association contributes to DNA organization. By using single molecular manipulation and imaging methods, we show here that distinct modes of non-specific DNA binding of IHF result in complex global DNA conformations. Changes in KCl and IHF concentrations, as well as tension applied to DNA dramatically influence the degree of DNA-bending. In addition, IHF can crosslink DNA into a highly compact DNA meshwork that is observed in the presence of magnesium at low concentration of monovalent ions, and high IHF-DNA stoichiometries. Our findings provide important insights how IHF contributes to bacterial chromatin organization, gene regulation, and biofilm formation.

TABLE OF CONTENTS

Table of Figures

CHAPTER 1: INTRODUCTION

1.1 BACTERIAL CHROMOSOMAL DNA ORGANIZATION

Bacteria are a large group of single-cell, prokaryote organisms (Fig. 1). The most apparent characteristic of bacterial cell is its small size. For example, *Escherichia coli* cell, a medium sized bacteria, is about 2 μm in length and 0.5 μm in diameter, with a cell volume of 0.6~0.7 μm^3 [1]. The most important structure in this small cell is the bacterial chromosome which contains many genes, regulatory elements and other nucleotide sequences. Unlike the eukaryotes, the bacterial chromosome is not confined to a membrane-enclosed nucleus but instead, is located inside the bacterial cytoplasm. The unstrained bacterial chromosomal DNA molecule is usually a couple of millimeters long. The *Escherichia coli* chromosome is one example. It has about 4.6M bp of genome with a linear length of about 1.6 mm [2]. When randomly coiled, it has a volume of about 200 μm^3, which is approximately 300 times larger than the entire volume of the cell. Therefore, the chromosomal DNA in bacteria has to be highly compacted to fit into the cell space. This compacting task in bacterial cell is executed by DNA supercoiling, macromolecular crowding and protein-DNA interactions [2].

It must be emphasized is that this highly compacted chromosomal DNA is not simply a disordered jumble but is in fact a well-organized and dynamic structure [3] which can be partially activated or deactivated rapidly during cell cycle or in response to environmental stimuli [2], such as the change of salt concentration, temperature or pH

value. There must be a sort of bacterial chromosomal DNA compaction which is effective only regionally and can be removed immediately. Protein-DNA interaction undoubtedly is the most suitable candidate to fulfill these functions, according to the way they modulate the DNA compaction.

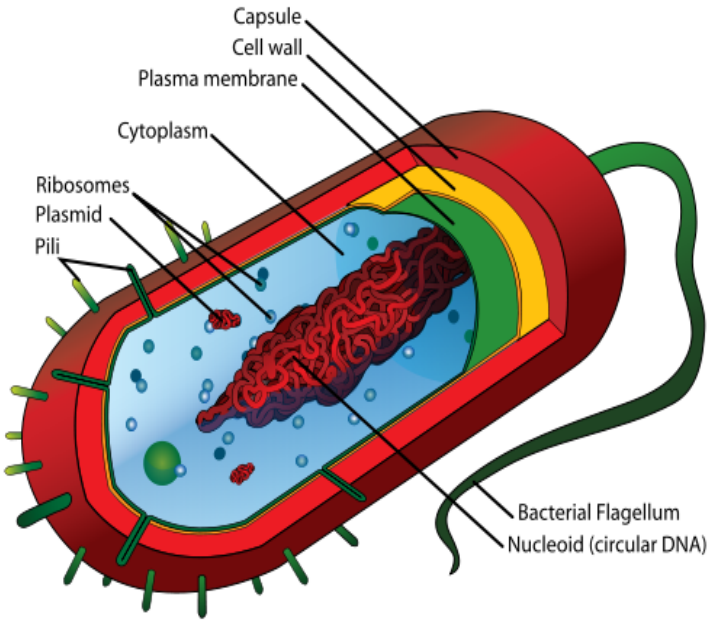

Figure 1. Schematic diagram of a bacterial cell (from *Anatomy and Physiology Resource Site which is free to copy under the license CC BY-NC-SA 3.0)*

1.2 NUCLEOID ASSOCIATED PROTEINS

Of all the bacterial chromosomes, *Escherichia coli* chromosome has been most studied. There are about 4000 protein species encoded by the *Escherichia coli* genome [4].

Approximately, 10% of them or more than 400 proteins, can be classified as DNA-binding protein. About 12 species of these DNA-binding proteins which include CbpA (curved DNA-binding protein A), CbpB (Curved DNA-binding protein B), DnaA (DNA-binding protein A), Dps (DNA-binding protein from starved cells), Fis (factor for inversion stimulation), Hfq (host factor for phage Q), H-NS (heat-stable nucleiod structuring protein), HU (heat-unstable nucleoid protein), IciA (inhibitor of chromosome initiation A), IHF (integration host factor), Lrp (leucine-responsive regulatory protein), and StpA (suppressor of td mutant phenotype A), are identified as the major DNA-binding proteins, which are also named as NAP (nucleoid-associated proteins) in *Escherichia coli* W3110 [4]. In 1999, Akira Ishihama's lab managed to measure the intracellular concentrations of these 12 proteins using the quantitative western blot method [4]. Moreover, a method termed genomic SELEX (Systematic Evolution of Ligands by EXponential enrichment) has been widely used in identifying the highest affinity sites of these nucleiod-associated proteins in the bacterial genome [5]. However, the molecular mechanisms of how these NAPs interact with chromosomal DNA are mostly unsolved, due to a lack of knowledge about the real-time measurement of individual protein-DNA interaction and the complexity of multiple protein-DNA interactions.

According to the numbers of bacteria, bacterial growth can be divided into four different phases: lag phase, log phase or exponential phase, stationary phase and death phase (Fig. 2A). In different growth phases, the conformations of bacterial chromosomal DNA are different. For example, the chromosomal DNA of *Escherichia coli* becomes more compact in the stationary phase [6]. Moreover, there is a great variation in NAP

intracellular abundance at different growth phases of *Escherichia coli* W3110 cell (Fig. 2B) [4]. In the exponential phase, the first 6 most abundant NAPs are Fis, Hfq, HU, StpA, H-NS and IHF, in order of abundance in descending order. In the early stationary phase, the order of abundance change to Dps, IHF, HU, Hfq, H-NS and StpA, while those in the late stationary phase are Dps, IHF, Hfq, HU, CbpA and StpA [4]. This dramatic difference might be an important factor in the compaction of the bacterial genome DNA and silencing of the bacterial gene at different growth phases [4]. Furthermore, different DNA-binding modes of these NAPs may play an important role in the organization and compaction of the bacterial chromosomal DNA.

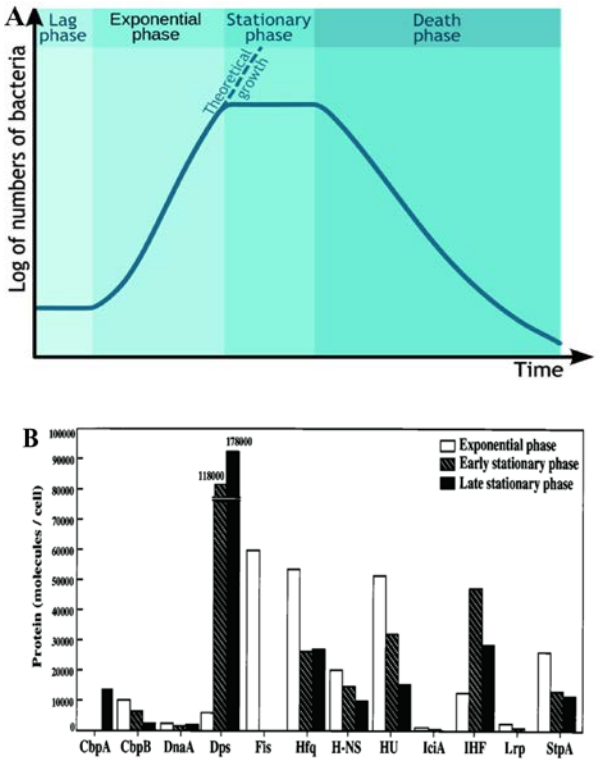

Figure 2. A) Bacterial growth phases.(from Wikipedia for the purpose to show bacterial growth phases) **B)** NAPs intracellular abundance at different growth phases of *Escherichia coli* W3110 cell [4] (with the permission of American Society for Microbiology).

In vitro investigations of purified individual NAPs by both single molecule and ensemble measurements suggest that there are four general binding modes of NAPs, which are bending, bridging, wrapping and clustering [3]. Some of these binding modes are showed in Fig. 3. For example, DNA bending by IHF by >160° with high affinity in a sequence-specific manner has been observed by the X-ray IHF-DNA crystal structure analysis [7]. Likewise, Dps, the most abundant protein in the stationary phase, which only appears in the stationary phase [4], compacts the DNA by clustering of distal DNA loci [4]. Interestingly, some NAPs can bind DNA in multiple modes. Take H-NS for example, it has been well-accepted that H-NS can cause DNA bridging. However, Yan Jie's group demonstrated that H-NS can also cause DNA stiffening by adjusting the divalent cations [8]. More examples and details of some major NAPs binding modes and their genome functions will be described in the next section.

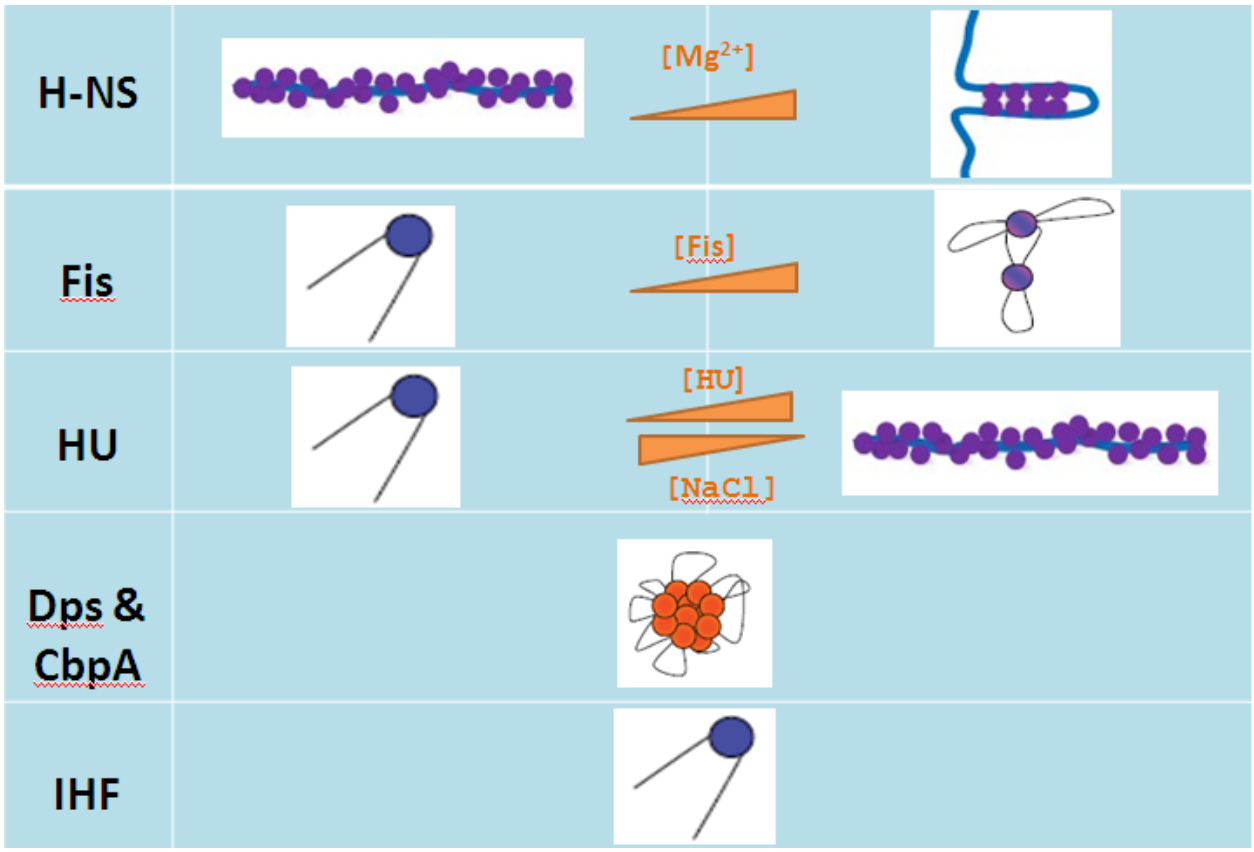

Figure 3 Some examples of NAP-DNA binding modes. 1) H-NS has been found to have two DNA binding modes, which are bridging DNA at high [Mg^{2+}] and stiffening DNA at low [Mg^{2+}]; 2) Fis has two binding modes: DNA-bending in low [Fis] and DNA-folding in high [Fis]; 3) under low [HU] and high [NaCl], HU causes DNA bending; otherwise HU causes DNA stiffening; 4) Dps and CbpA were found to cause DNA condensation; 5) IHF has been found to bend DNA by specific DNA-binding.

.

1.3 CURRENT UNDERSTANDING OF MAJOR NAPS: HU, FIS, H-NS AND IHF

1.3.1 HU

Heat-unstable nucleiod protein (HU) consists of two subunits, HUα and HUβ, which have 70% similarity in amino acid sequence [9]. HU can form either homodimer or heterdimer at different growth phases of the *Escherichia coli* cell [9]. In the exponential growth phase, there are about 30,000 to 55,000 HU in the *Escherichia coli* W3110, suggesting that HU is a major nucleoid protein in the growing bacterial cell [4].

HU-DNA interactions were thought to be nonspecific; however, it was found to be more likely to bind to the distorted DNAs, which has high superhelical density [9]. HU-DNA crystal structure shows that HU introduces a 105° ~ 140° bending on DNA [7]. Besides this, HU reduces the DNA effective stiffness at low protein concentrations and increases it at high protein concentrations [9]. All these HU-DNA binding properties are consistent with its role in bacterial chromosomal genome recombination and DNA topology arrangement. There are many data showing that HU plays an important role in the expression of many genes in *Escherichia coli*, such as central metabolism and respiration [9].

1.3.2 FIS

Factor for inversion stimulation (Fis) is the most abundant nucleiod associated proteins in the growing *Escherichia coli* cell, when its intracellular concentration reaches up to 60,000 molecules per cell. However, it is almost undetectable during the stationary phase [4].

Fis interacts with DNA in a number of ways, causing DNA wrapping, bridging and bending [9]. Fis-DNA interactions seem to be specific. It binds as a homodimer to the DNA sequence that is commonly 17bp in length and AT rich, except at positions 2 and 16, where C or G residues are usually found [9].

Consistent with its multiple DNA interaction modes, Fis takes part in many gene regulation and genome organization processes. For example, Fis is a traditional transcription activator, which makes physical contact with RNA polymerase [10]. Moreover, Fis can activate or deactivate promoters, relying on its binding site location relative to that of RNA polymerase [9].

1.3.3 H-NS

Heat-stable nucleoid structuring protein (H-NS) reaches a maximum of about 20,000 copies per cell in the exponential phase, but it decreases to 40% of the maximum at the late stationary phase [4]. It exists as a dimer or high-order oligomer [8]. H-NS preferentially binds to A-T rich DNA [11], in that way that it forms dimer in N-terminal domain whereas it binds DNA in C-terminal domain [8].

H-NS bridging DNA is a well-accepted mode which was thoroughly described by Remus Dame and his coworkers [12]. However, a recent study in Yan Jie's group shows that H-NS can also cause DNA stiffening; and these two modes can be switched by adjusting

divalent metal ions [8]. The stiffening binding mode might be highly correlated with its role in gene silencing, whereas the bridging binding mode might be most relevant to its function in nucleoid compaction [8].

1.3.4 IHF

The integration host factor (IHF) protein is a highly conserved abundant nucleoid associated protein (NAP) in all the growth conditions and growth phases of bacteria [13]. It was originally discovered as an essential co-factor for the site-specific recombination of λ phage in the *E.Coli* genome (Fig. 4A) [14]. This function requires binding of IHF to highly specific DNA sequences, and its role is to create a sharp bending angle (>160 degree) at its binding site (Fig. 4C) [15]. Later, it was also identified as a transcription factor that influences global gene transcription in both *E. Coli* [16] and *S. Typhimurium* [17, 18] (Fig. 4B). It has been suggested that its gene regulatory role is also related to its sharp DNA bending capability, by which it can positively regulate gene transcription in facilitating contact between regulatory proteins and RNA polymerase [19].

Analysis of IHF site-specific sequences has revealed consensus DNA-binding motif consisting small clusters of conserved bases [20-22]. IHF binds to its specific binding sequences with an affinity significantly stronger than its binding to non-specific sequences [23-25]. One example is the H' sequence in λ phage [26, 27], which has been determined to have a dissociation constant in ~100 mM KCl in the range of 2 - 20

nM by earlier titration assays [23-25] and 0.01 – 0.1 nM by recent kinetic measurement [28].

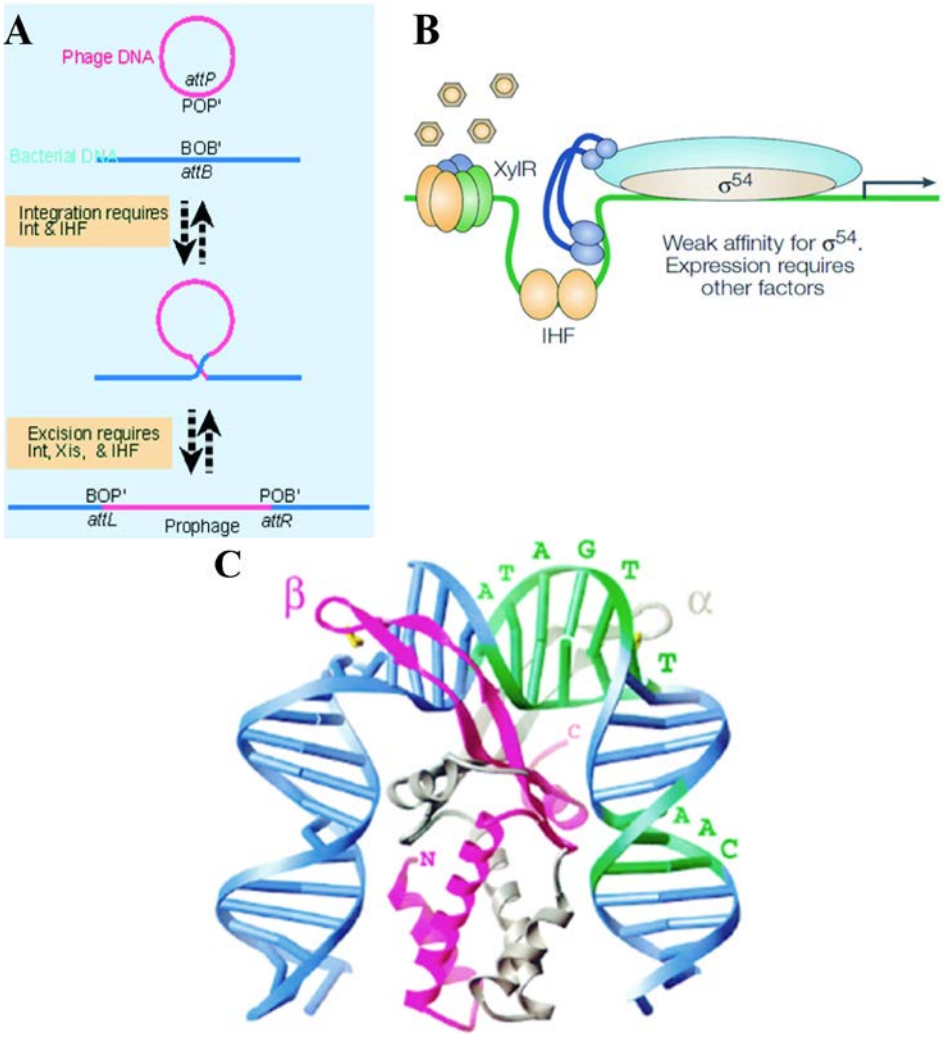

Figure 4. Specific Functions of Integration Host Factor (IHF). **A)** IHF is an essential co-factor for the site-specific recombination of λ phage in the *E.Coli* genome (from GeneVIII). **B)** IHF is a transcription factor [18] (with the permission of Nature Publishing Group). **C)** Specific binding of IHF induces sharp DNA bending [15] (with the permission of ELSEVIER LICENSE).

In contrast to the high affinity of IHF to its specific binding sequences, the intracellular concentration of IHF is significantly larger than its specific K_D in all the growth phases. IHF is highly abundant, with a copy number ranged from 12,000 in the exponential growth phase and 55,000 in the early stationary phase, which translate into a concentration range of 12 – 55 μM [29]. Such a high concentration suggests that IHF may also play a role beyond its site-specific recombination and specific gene regulations through non-specific DNA binding.

1.4 DNA AND NAPS IN EXTRACELLULAR POLYMERIC SUBSTANCES (EPS) OF BIOFILMS

As illustrated before (Section 1.3), nucleoid associated proteins (NAP) play an important role in intracellular bacterial chromosomal DNA organization and gene regulation. Moreover, some of the NAPs, such as IHF and HU, are also found present in the extracellular polymeric substances (EPS) of biofilms [30].

In nature, bacteria live in the form of biofilms in which many bacteria form an organized, functional, complex community. The major component of the biofilm is the extracellular polymeric substances (EPS) that mainly contain polysaccharides, proteins, nucleic acids and lipids [31]. In the EPS, extracellular DNA (eDNA) is a common component and forms a complex DNA meshwork. It has been demonstrated that the eDNA meshwork plays an important role in stabilizing the biofilms [32].

Recent study shows that IHF and HU are found in the eDNA meshwork [30, 33], which are located at both kinked DNA and crossed DNA within an NTHI biofilm (Fig. 5) [33]. This study also indicates that IHF and HU are critical for the integrity of the EPS matrix of biofilms: removal of these proteins either leads to biofilm disassembly or biofilm debulking [33].

However, despite the potential importance in the biofilms, very little is known about how these NAPs, such as IHF and HU, organize DNA and how they responses to environmental factors.

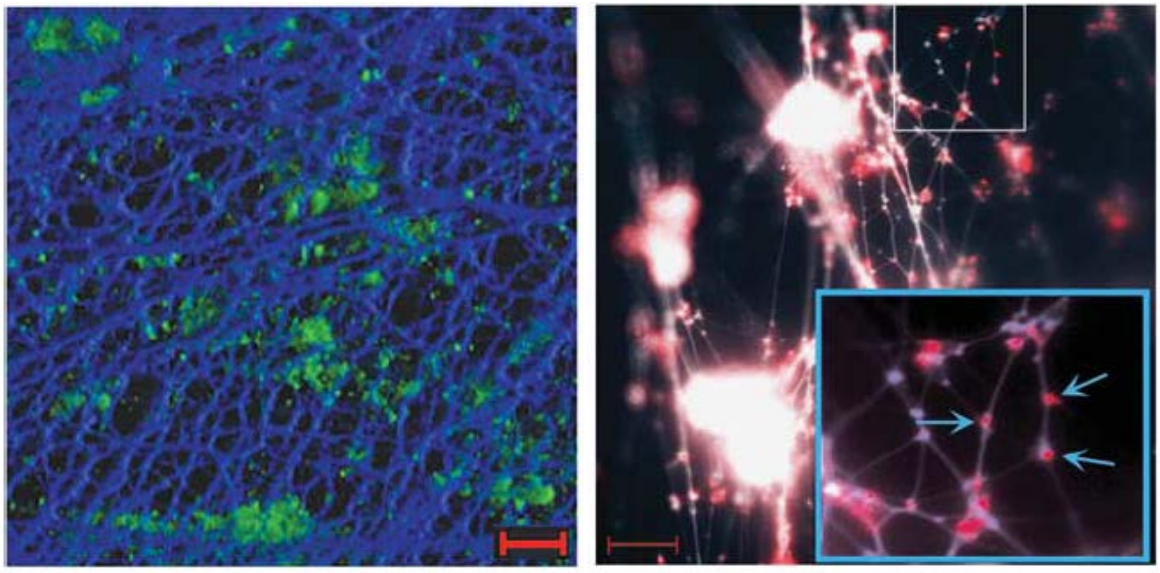

Figure 5. Extracellular DNA meshwork bound by non-specific binding of IHF and HU [33] (for the purpose to show e-DNA meshwork with IHF and HU) (with the permission of Creative Commons License).

1.5 QUESTIONS RAISED AND THE MOTIVATIONS

The effects that non-specific binding of IHF to DNA have on the mechanical properties of DNA have been studied in a single-DNA stretching experiment for 48,502 bp of λ–DNA [21]. It was found that addition of IHF weakly reduced DNA extension at the saturation binding concentration of > 500 nM IHF [21]. In that experiment, the effect of IHF binding on the force response of DNA is similar to that predicted for proteins that can bend DNA [34, 35], suggesting that non-specific binding of IHF also bends DNA. However, it is not clear whether the non-specific binding of IHF to DNA introduces a sharp angle, like that induced by specific binding of IHF to the H' sequence [15]. It appears that at saturation binding, less DNA bending observed than expected in that experiment [34, 35]. This observation suggests that either non-specific binding of IHF only introduces weak DNA bending under the conditions used, or that it can introduce sharp DNA bending, but only sparsely binds to DNA even at its saturation binding concentration. Furthermore, many bacterial NAPs, such as H-NS and StpA, can sense environmental changes and consequently change their DNA binding properties [8, 36]. It is unclear how IHF environmental factors influence the DNA binding properties of IHF.

In this study, the non-specific interaction between IHF and DNA was investigated by single-DNA manipulation using magnetic tweezers and atomic force microscopy (AFM). Our results reveal multiple non-specific DNA binding modes of IHF, resulting in complex DNA structures, which can be altered by changes in conditions such as protein concentration, monovalent salt concentration, and magnesium concentration.

CHAPTER 2: METHODS AND MATERIALS

2.1 MICROMECHANICS OF DNA AND ITS FORCE RESPONSE

2.1.1 STRUCTURE OF DNA DOUBLE HELIX

Deoxyribonucleic acid (DNA) is a long biopolymer constituted by repeating units called nucleiotides which carries the genetic materials of all living organisms except RNA viruses. In 1953, Watson and Crick first proposed the structure of DNA as the form of a double helix by the X-ray diffraction data [37]. As illustrated in Fig. 6A), DNA consists of two polynucleotide strands, with backbones constituted by 5-carbon sugars and phosphoric acid groups joined by ester bonds. These two chains run in opposite directions - which is named as antiparallel - connected by hydrogen bonding between the nitrogenous bases which are attached to the 5-carbon sugars. Adenine (A) pairs specifically with thymine (T) while guanine (G) pairs specifically with cytosine (C). The bonding is called base pairing and the paired bases are described as complementary.

To stabilize the whole DNA structure, there are two kinds of interactions to make the two chains twist around each other- one is the inter-chain “base-pairing” which holds the two complementary chains together; the other is the intra-chain “stacking” which connects between adjacent bases.

DNA has many possible conformations, such as A-form DNA, B-form DNA and Z-form DNA. However, B-form of DNA is the most common conformation found in cells. The B-form DNA double helix is right-handed as shown in Fig 6 B. The distance between two neighboring bases is about 3.4 Å. Each base pair rotates approximately 36° ; so around 10.3 base pairs make a full turn. The interwinding of the two chains forms two kinds of grooves; the major groove, is 22Å wide and the minor groove, is 12Å wide.

It is important to realize that the B-form of DNA is a dynamic structure. The individual base pairing energy ranges from $1k_BT$ to 4 k_BT, depending on the DNA sequence, at room temperature. As the most important component in the cell, DNA undergoes thermal fluctuations from its surrounding, usually in the order of several k_BT at room temperature. Consequently, its base pairs undergo open-close fluctuations all the time.

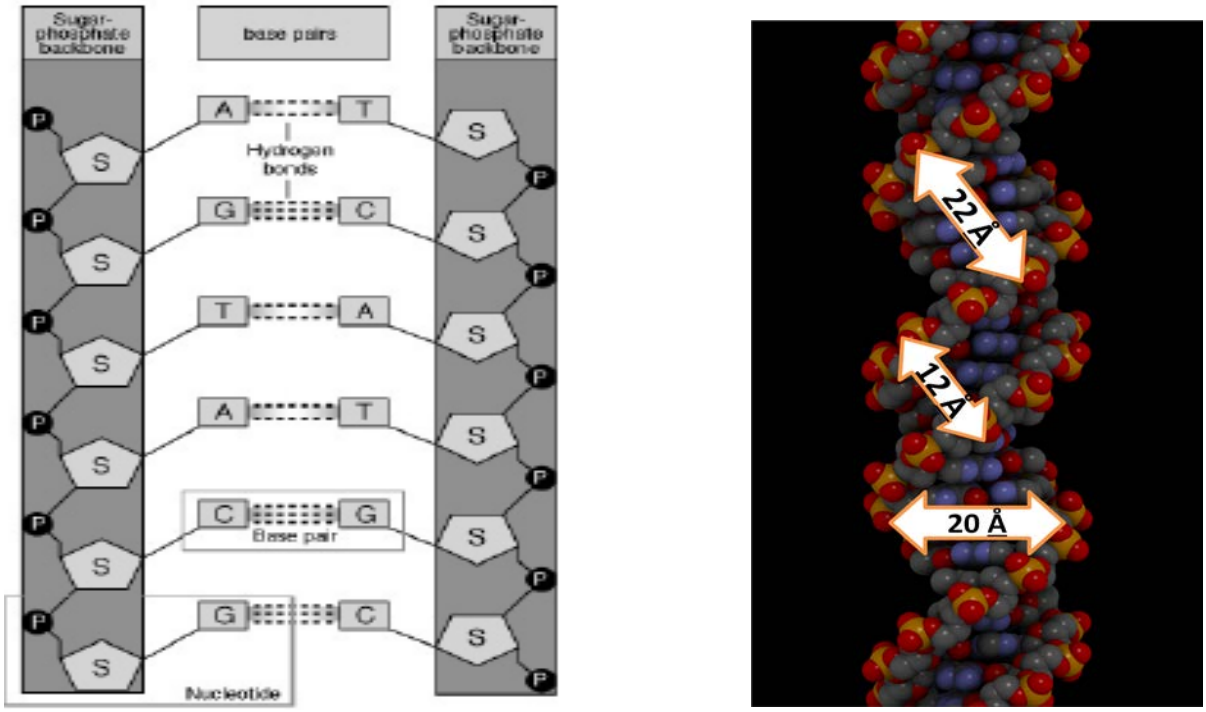

Figure 6. A) Schematic structure of DNA backbone (from GeneVII). **B)** Schematic structure of B-form of DNA (generated by Qutemol).

2.1.2 WORM-LIKE-CHAIN (WLC) MODEL

As described in the last section, DNA is basically a very long cylinder with a very small diameter, about 2 nm, compared to its contour length. One base-pair, the single unit of DNA, is only 0.34 nm long, is also much smaller than its entire length. Therefore, it might be possible that the dynamic properties of DNA may not rely on its microscopic structure. Consequently, some simple models with a few phenomenological parameters might be able to simplify this system, and describe this system properly.

One of these models is named as Freely-Jointed-Chain (FJC) model. As illustrated in Fig.7, DNA is modeled as a chain of N concatenated rigid independent segments, each with the length b, which is called Kuhn length. The orientations of each segment are uncorrelated in the absence of an external force [38]. When we apply a force f $\hat{z}$ on the DNA chain, the effective energy E for the chain is shown as below

$$\frac{E}{\mathrm{k_B T}} = \sum_{i=1}^{N} \frac{fb}{k_B T}\, \widehat{t_\iota} \,.\, \hat{z} \qquad (1)$$

where k_B is Boltzmann's constant, T is temperature, $\widehat{t_\iota}$ is tangent vector of the i^{th} segment. From (1), the end-to-end distance of the polymer can be analytically derived [38]:

$$< z > = L \left(\coth \frac{fb}{\mathrm{k_B T}} - \frac{\mathrm{k_B T}}{\mathrm{fb}} \right) \qquad (2)$$

where L is DNA contour length.

At low force, FJC model behaves as a simple spring, which can fit DNA elasticity very well. However, at high force, this model predicts that the DNA end-to-end extension scales with the force as $\frac{\mathrm{k_B T}}{\mathrm{fb}}$, which fails to explain the experiment data of DNA. Instead, it was found in the experiments that DNA extension scales with force as $\left(\frac{\mathrm{k_B T}}{\mathrm{fb}}\right)^{\frac{1}{2}}$ [39, 40].

The DNA force-response was found to be consistent with the Worm-Like-Chain (WLC) model that assumes DNA is a homogeneous inextensible polymer with a finite bending stiffness. The WLC mode is actually very similar to FJC model, but changes from independent segments to a continuous elastic medium [39, 40]. Fig. 8 is a schematic diagram of this WLC model. The effective energy E for the chain is given by

$$\frac{E}{k_B T} = \int_0^L \left[\frac{A}{2} \left| \frac{d\,\widehat{\boldsymbol{t}(s)}}{d\,s} \right|^2 - \frac{f}{k_B T}\,\widehat{\boldsymbol{t}(s)} \cdot \hat{z} \right] ds \qquad (3)$$

where *s* is the contour position along DNA, *A* is the persistence length of DNA, over which the tangent vector correlations dies off along the DNA chain. It is also related to the bending rigidity of DNA, *B,* by the relation $A=B/k_BT$. In physiological buffer conditions, *A* has been determined by single-DNA stretching experiments and DNA looping experiments to be about 50 nm or 150 bp [39, 40].

This continuous WLC model can also be transformed into discrete form if the segment length *b* is much smaller than the persistence length *A*:

$$\frac{E}{k_B T} = \sum_i^{N-1} \left[\frac{A}{2b} \left(\widehat{\boldsymbol{t_{i+1}}} - \widehat{\boldsymbol{t_i}} \right)^2 - \frac{fb}{k_B T}\,\widehat{\boldsymbol{t_i}} \cdot \hat{\boldsymbol{z}} \right] \qquad (4)$$

where $\widehat{t_i}$ is tangent vector of the ith segment.

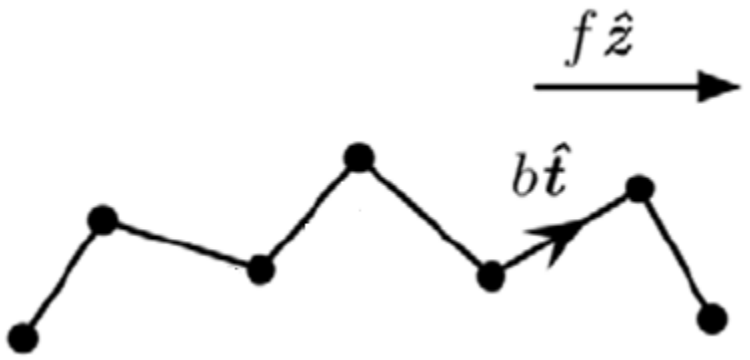

Figure 7. Schematic of FJC model. In this model, DNA is modeled as a chain of N concatenated rigid independent segments, each with the length b, called Kuhn length.; $\hat{t}$ is tangent vector; f is the force which in the direction of $\hat{Z}$.

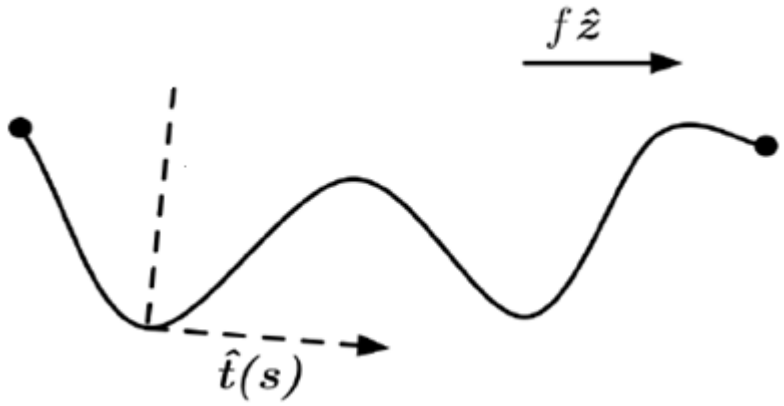

Figure 8. Schematic of WLC model. In this model, DNA is a homogeneous inextensible polymer with a finite bending stiffness. f is the force which in the direction of $\hat{Z}$; *s* is the contour position along DNA; $\hat{t}$ is tangent vector.

2.1.3 FORCE-EXTENSION CURVE OF DNA

The analytic solution of the force-extension relation of Worm-Like-Chain model is not available now, but the numerical solution has been figured out [39, 40]. It is called Marko-Siggia formula, as shown below

$$\frac{fA}{k_B T} = \frac{1}{4}\left(1 - \frac{z}{L}\right)^{-2} - \frac{1}{4} + \frac{z}{L} \qquad (5)$$

When the force is much larger than $\frac{k_B T}{A}$ (which is about 0.08pN) and smaller than 15pN, this formula fits DNA experiment data very well, compared with FJC model. This can be clearly identified in Fig. 9: squares are the experiment data for 97004 bp lambda DNA dimmers in 10 mM Na+ buffer; solid curve is a fit by the asymptotic Marko-Siggia formula for A=53 nm and L=32.8 um; dashed line the is a fit by FJC model for b=100 nm and L=32.7um [39, 40]. We can see that in the small force range, both FJC and WLC are consistent with the experimental data but in the higher force range, DNA extension scales with force as $\left(\frac{k_B T}{fb}\right)^{\frac{1}{2}}$; therefore only WLC model fits the experimental data.

However, when the force is above ~15 pN, using the WLC model becomes problematic. This is because WLC assumes an inextensible polymer, where the entire chain length is constant. The DNA structure is however not stable under the above condition as it is deformed from its normal B-form DNA. An extreme example is when the force is approximately 60 pN, DNA undergoes overstretching phase transition with its contour length extended to 1.7 times the B-form DNA [41].

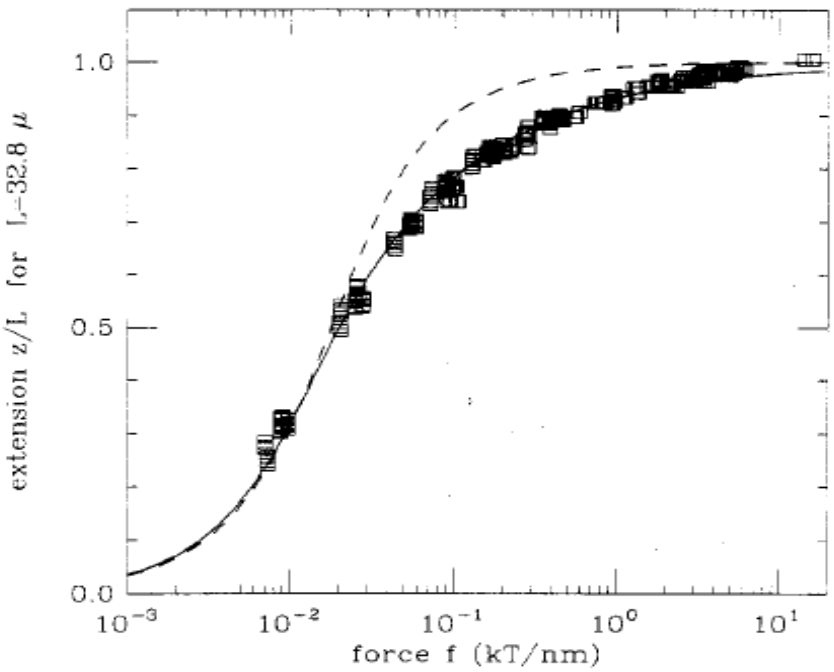

Figure 9. Fits of Marko-Siggia formula and FJC formula to experimental data of Smith et al. [40] (with the permission of American Chemical Society Publications)

2.1.4 EFFECTS OF DNA-DISTORTING PROTEINS ON DNA FORCE-RESPONSE

As mentioned in Chapter 1, there are many DNA binding proteins inside the bacterial cell which can bend, stiffen, bridge, compact or lengthen the DNA target. For example, H-NS can introduce two kinds of interactions to DNA - bridging and stiffening [8]; while HU and IHF both introduce large bends into DNA structure [7, 15]. To date, plenty of experimental papers studying the effects of these DNA-distorting proteins on DNA

elastic response have been published. Most of them focused on the sequence-specific interactions between these DNA binding proteins and DNA by electrophoretic gel study, because short, defined DNA can be used and the band shift can be well-measured after the protein binding [34]. However, most of these DNA–binding proteins can interact with bacterial chromosomal DNA non-specifically. Single-molecule manipulation techniques such as magnetic tweezers, optical tweezers and atomic force microscopy, have appeared as powerful tools to study the fore-extension response of DNA-protein composites. Therefore, we need a well-defined model to quantify these experimental data using more lucid parameters, such as the protein bound site occupation, binding free energy etc.

In 2003, Yan Jie and John Marko published a theoretical study of the bending, stiffening and lengthening effects of DNA-binding proteins on DNA force-extension response [34]. They used the discrete Worm-Like-Chain (WLC) model (see Formula 4 in section 2.1.2 for details) and transfer matrix to describe the protein-DNA complex. Since their study is very useful to calculate the protein-binding occupation of my IHF non-specific binding experiment data, the principle and major simulation results of their research will be discussed in the rest of this section.

EFFECTS OF DNA-BENDING PROTEINS

In this model, DNA is considered as a long chain of N segments with the length b, energy $\boldsymbol{E_i}$. When a protein is bound to one segment, it forces a bend by an angle φ (see Fig. 10 for more details). The total energy is given by [34]

$$\boldsymbol{E} = \sum_{i=1}^{N} \boldsymbol{E_i} \qquad (6)$$

where the energy of i[th] segment , i.e. $\boldsymbol{E_i}$ is

$$\frac{\boldsymbol{E_i}}{\mathrm{k_B T}} = \frac{\boldsymbol{a}}{\boldsymbol{2}} |\widehat{\boldsymbol{t_i}} - \widehat{\boldsymbol{t_{i-1}}}|^2(\boldsymbol{1} - \boldsymbol{n_i}) + \left[\frac{\boldsymbol{a'}}{\boldsymbol{2}} (\widehat{\boldsymbol{t_i}} . \widehat{\boldsymbol{t_{i-1}}} - \boldsymbol{\gamma})^2 - \boldsymbol{\mu}\right] \boldsymbol{n_i} - \frac{\boldsymbol{bf}}{\boldsymbol{2}} (\widehat{\boldsymbol{t_i}} + \widehat{\boldsymbol{t_{i-1}}}) . \hat{\boldsymbol{z}} \qquad (7)$$

where $\mu = \cos\varphi,$ is the binding free energy; a is the bending stiffness of bare DNA; $\boldsymbol{a'}$ is bending stiffness of DNA-protein composite, $\widehat{t_i}$ is the tangent vector of segment i; f is the applied force which is along $\hat{z}$ direction.

There are two kinds of bending described in this paper: one is called stiff bending, which means the bound protein will leave from the DNA under large force; the other is named as flexible bending, under which condition the protein-DNA complex will deform at large force. Fig. 11a is the force-extension curve of the stiff 90° ($\boldsymbol{\gamma = 0}$) bending ($\boldsymbol{a' = 100}$) with different binding strengths $\mu = -\infty\ (bare\ DNA), -2.3, -1.61, -0.69 \text{respectively} 9, 0, 3\ and\ 6.$, while Fig. 11b describes those of the 90° ($\boldsymbol{\gamma = 0}$) flexible bending ($\boldsymbol{a' = 2}$) with different $\mu = -\infty, -2.3, -1.61, -0.69, 0, 3$ respectively. At small binding free energy, the curves of stiff and flexible bending are similar. At large binding strength, abrupt extension

increases appear at large force in stiff bending cases due to the sudden unbinding of the protein, whereas this cannot be observed in flexible bending [34].

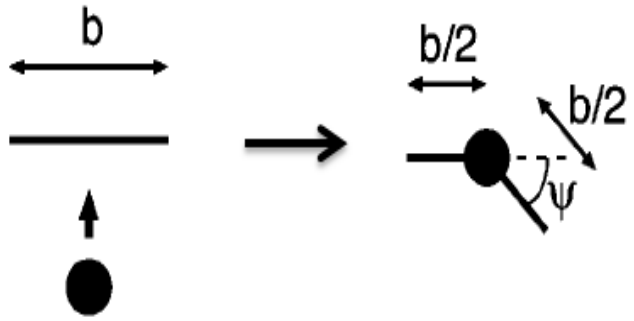

Figure 10. Schematic of the model for DNA –bending proteins [34]. (Figures used by courtesy of author Dr. Yan Jie)

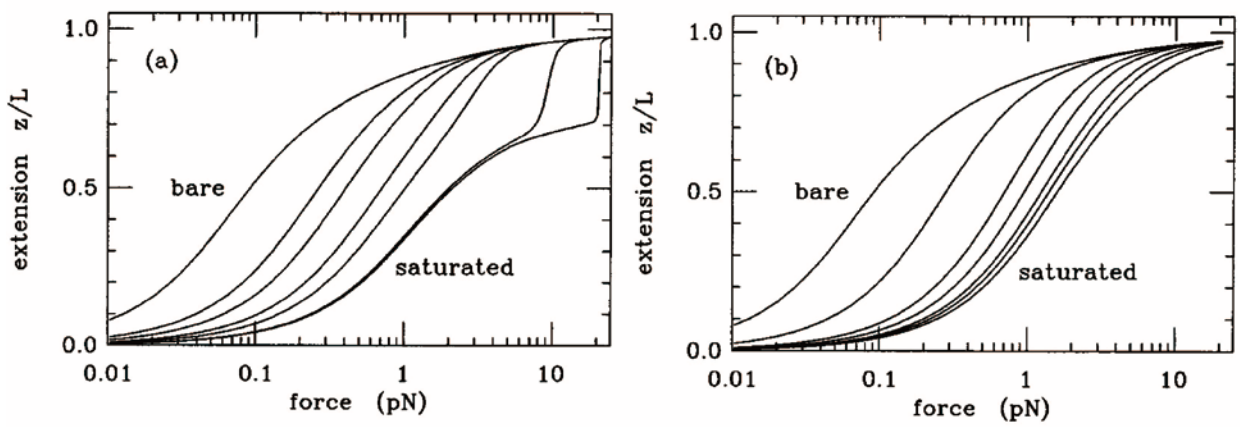

Figure 11. a) Force-extension curve of the stiff 90°($\boldsymbol{\gamma = 0}$) bending ($\boldsymbol{a' = 100}$) with different binding strengths $\mu = -\infty, -2.3, -1.61, -0.69, 0, 3\ and\ 6.91$. **b)** Force-extension curve of the 90°($\boldsymbol{\gamma = 0}$) flexible bending ($\boldsymbol{a' = 2}$) with different $\mu = -\infty, -2.3, -1.61, -0.69, 0, 3$. [34] (Figures used by courtesy of author Dr. Yan Jie)

EFFECTS OF DNA-STIFFENING PROTEINS

When stiffening proteins bind to DNA, they do not bend the DNA, but instead change the bending constant of the DNA backbone. In this case, $\boldsymbol{E_i}$ is given by

$$\frac{E_i}{k_B T} = \frac{a}{2}\,|\hat{t}_i - \widehat{t_{i-1}}\,|^2(1 - n_i) + \left[\frac{a'}{2}\,|\hat{t}_i - \widehat{t_{i-1}}|^2 - \mu\right] n_i - \frac{bf}{2}\,(\hat{t}_i + \widehat{t_{i-1}})\,.\,\hat{z} \qquad (8)$$

where a' is the bending constant after the protein binding [34].

Fig. 12 [34] shows the force-extension curves of this model when b=5nm, a=10 and $a' = 100$. Compared to the rightmost curve of bare DNA ($\mu = -\infty$), the extension of DNA-stiffening protein complex is always larger under the same force, which is even more obvious at small force. This is because of the effect of stiffening proteins binding which increases the stiffness of DNA.

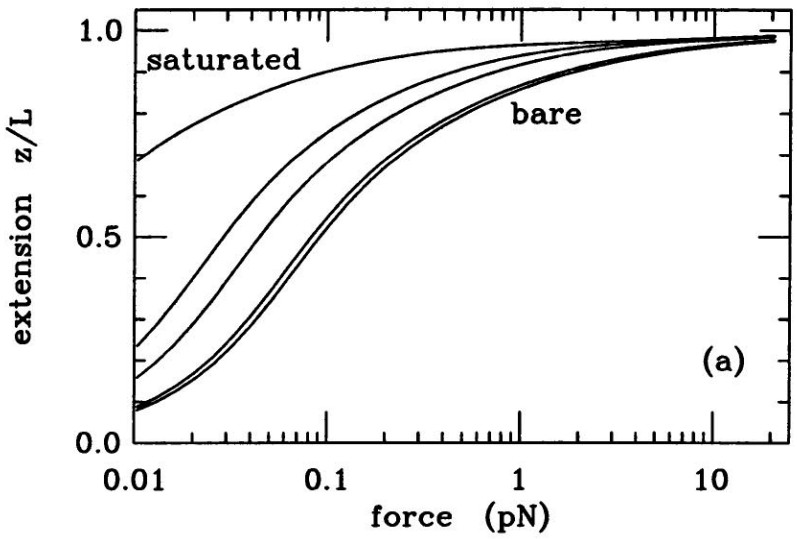

Figure 12. Force-extension curves of DNA and DNA-stiffening protein complex with different binding strengths $\mu = -\infty\ (rightmost\ curve, corresponding\ to\ naked\ DNA)$, $0, 2.3, 3\ and\ 4.6$ (b=5 nm, a=10; $a^{'} = 100$) [34]. (Figure used by courtesy of author Dr. Yan Jie)

EFFECTS OF DNA-INTERCALATING PROTEINS

When DNA-intercalating proteins bind to DNA double helix, they stretch the DNA and change the DNA bending constant without introducing any kinks. Plenty of proteins and drugs belong to this category, such as ethidium bromide and YOYO. In this case, $\boldsymbol{E_i}$ is given by

$$\frac{E_i}{k_B T} = \frac{a}{2}\,|\hat{t}_i - \widehat{t_{i-1}}\,|^2(1 - n_i) + \left[\frac{a'}{2}\,|\hat{t}_i - \widehat{t_{i-1}}|^2 - \mu\right] n_i - \frac{bf}{2}(1 + \alpha n_i)\,(\hat{t}_i + \widehat{t_{i-1}})\,.\,\hat{z} \qquad (9)$$

The force-extension curves of this model with different binding strengths is illustrated in Fig. 13, when b=5nm, a=10,$a^{'} = 40,\ \alpha = 0.5\ [30]$. In this situation when intercalating proteins are fully occupied on DNA backbone, the DNA contour length increases to 1.5 times its original contour length.

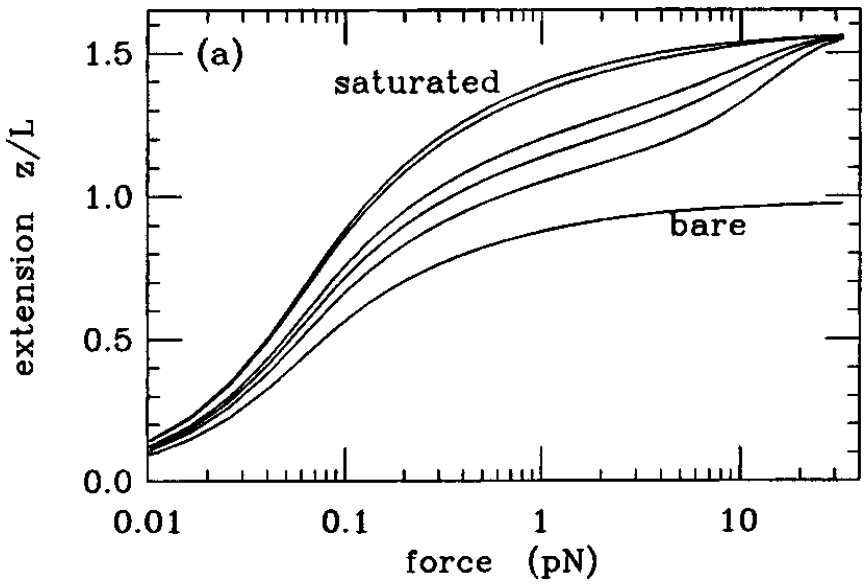

Figure 13. Force-extension curves of DNA and DNA-intercalating protein complex with different binding strengths $\mu = -\infty\ (rightmost\ curve, corresponding\ to\ naked\ DNA), -1.20, -0.51, 0, 2.3\ and\ \infty$(b=5nm, a=10; $a^{'} = 40, \alpha = 0.5$) [34]. (Figures used by courtesy of author Dr.Yan Jie)

2.2 SINGLE-MOLECULE MANIPULATION BY MAGNETIC TWEEZERS

2.2.1 SINGLE-MOLECULE MANIPULATION TECHNIQUES

Single-molecule manipulation has become increasingly important over the last 20 years. It consists of atomic force microscopy (AFM), optical tweezers (OT), magnetic tweezers (MT), micro-needle manipulation, flow-induced stretching and biomembrane force probe [42]. The first three are the most widely used techniques.

Compared to the traditional bulk methods, single-molecule manipulation avoids ensemble average measurement over all accessible molecules. Instead, it provides real-time “single-molecule” measurement of biological events which can be captured often enough to make sure that they are not trivial and artificial. Similarly, single-molecule techniques are very suitable to study many complicated biological processes which usually includes multistate and multispecies [42]. Moreover, external force which has a crucial role in many biological processes can be accurately exerted. It can span six orders of magnitude (from 10000pN to 0.01pN) in single-molecule manipulation [42].

In my study, transverse magnetic tweezers (TMT), which is an important member of magnetic tweezers family, are frequently used to get real-time force-extension spectroscopy of DNA-IHF composite. Its operating principles and practical implementation will be discussed in section 2.2.2 and 2.2.3. Atomic force microscopy (AFM) was used to give the 3D images of DNA-IHF complex in different buffer conditions, which will be described in section 2.3. In the rest of this section, other major

single-molecule manipulations methods such as optical tweezers (OT) and vertical magnetic tweezers (VMT) will be introduced.

OPTICAL TWEEZERS (OT)

Optical tweezers (OT) also known as single-beam gradient force trap, are able to manipulate nanometer to micrometer sized dielectric particles by exerting a force ranging from 0.1 piconewton to 100 piconewton via a highly focused laser beam. It can provide three-dimensional displacement of the trapping particle down to sub-millisecond time resolution and sub-nanometer accuracy [42]. Due to all these features, optical tweezers have been widely used in the research of a variety of biological systems.

The operating principle of optical tweezers is illustrated in Fig. 14. The beam waist, which is the narrowest region of the focused laser beam, creates an optical trap with an intensive electric field gradient. Dielectric particles in this beam waist region undergo a restoring force along the direction of the gradient. For small displacements of the trapped particles from the trap center, the restoring force is linearly proportional to its displacement. In this situation, this optical trap can be described as a simple spring, which obeys Hooke's law. Particles with size ranging from ~20nm to a few micrometers can be trapped effectively. Accordingly, organelles, single cells, lipid vesicles and silica

or polystyrene beads with attached biological molecules can be manipulated by optical tweezers [42].

However, optical tweezers have some limitations. Photodamage and sample heating are the two major drawbacks which should be considered before and during usage.

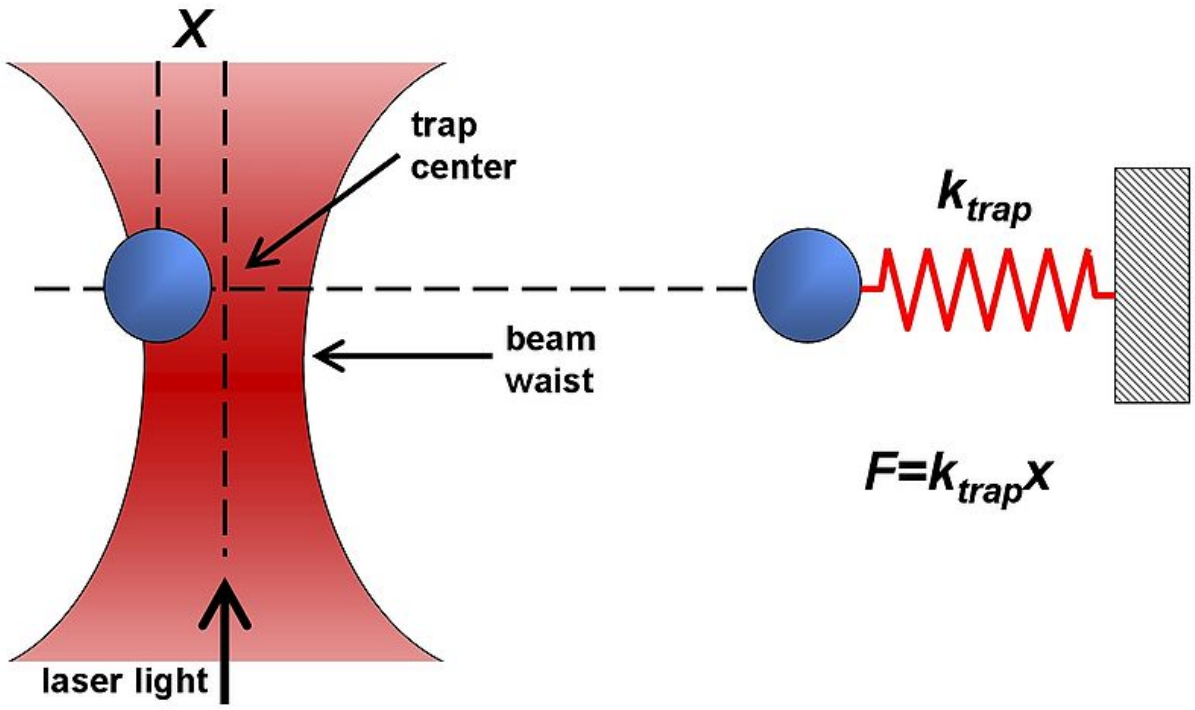

Figure 14. Schematic diagram of optical tweezers operating principle (from wikipedia).

VERTICAL MAGNETIC TWEEZERS (VMT)

Magnetic tweezers are a powerful tool to study biological processes. Compared to other single-molecule manipulation techniques, magnetic tweezers have many advantages such as no sample heating unlike the optical tweezers; specificity compared with AFM, and throughput and force stability compared with both AFM and optical tweezers [43, 44].

Vertical magnetic tweezers (VMT) are the traditional type of magnetic tweezers. In 1992, Smith's lab used a combination of hydrodynamic flow and magnets to study DNA elasticity for the first time [38]. After that, this method was improved by Strick et.al. by eliminating hydrodynamic flow to improve the signal-to-noise ratio [38]. In VMT apparatus, as shown in Fig. 15, a molecule which can either be DNA or protein is attached to a glass slide on one end and a magnetic bead on the other by some specific interactions between the modified DNA end and the functionalized glass or bead surface. A pair of magnets is used to create a magnetic field near the studied molecule. Because of the linked magnetic bead, a stretching force is exerted on the molecule which is perpendicular to the glass surface, i.e. along Z direction. The force can be measured by the bead's thermal fluctuations, with the formula as below

$$F = \frac{\mathrm{k_B T\, z}}{\delta y^2}, \qquad (10)$$

where k_B is Boltzmann's constant, T is temperature, z is the extension of the tether, δy^2 is the variance of thermal fluctuations in the direction perpendicular to the magnetic field lines.

Previously, vertical magnetic tweezers are only used to study long molecules (>1μm) with the force ranging from 1pN to over 100pN because it is difficult to measure force in high force region (>20pN) for the short tethers (<1μm). This limitation was solved in Hu Chen's newly published paper [44]. By analyzing the y-fluctuation of the bead and combining to the magnetic field-to-distance exponentially decay formula, they used magnetic tweezers to stretch DNA or protein as short as 100nm in length with accurate force calibration over a wide range up to 100pN [44]. Therefore, the application of vertical magnetic tweezers has been expanded to many new fields, such as short DNA overstretching and protein unfolding/refolding.

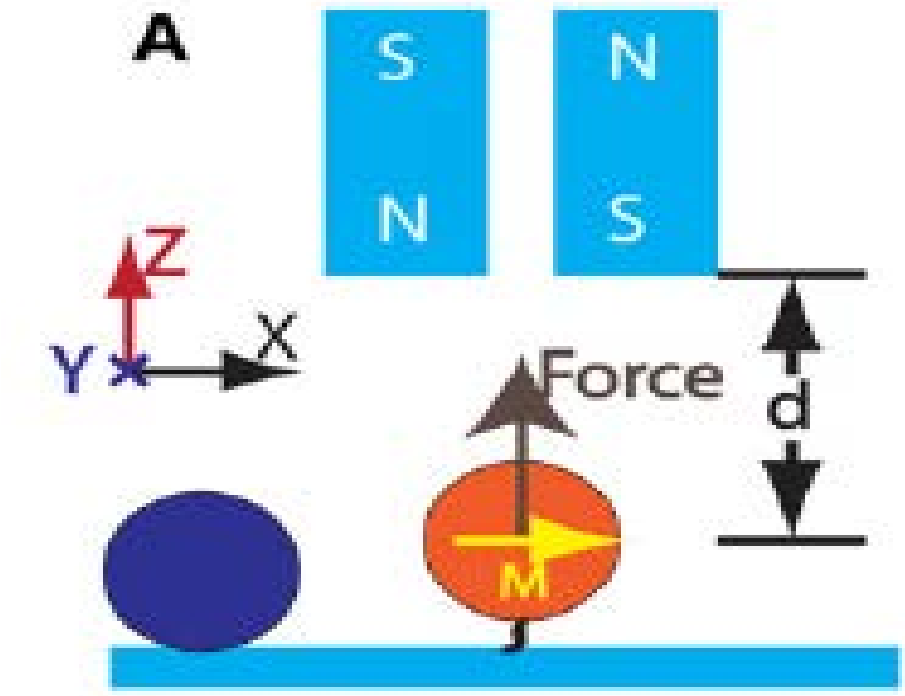

Figure 15. Schematic diagram of vertical magnetic tweezers apparatus [44]. In this set-up, a molecule which can either be DNA or protein is attached to a glass slide on one end and a magnetic bead on the other end. A pair of magnets is used to create a magnetic field near the studied molecule. Because of the linked magnetic bead, a stretching force is exerted on the molecule which is perpendicular to the glass surface, i.e. along Z direction. (with the permission of Elsevier)

2.2.2 TRANSVERSE MAGNETIC TWEEZERS USED IN THE STUDY

Conventional magnetic tweezers, i.e. vertical magnetic tweezers, stretch the molecule perpendicular to the objective focal plane and measure the tether extension change either by calibrations of the out-of-focus bead images or dynamic refocusing [45]. This indirect extension measurement makes the data analysis complicated and inaccurate;

what's worse, it limits the traditional magnetic tweezers to the study of short molecules shorter than 3μm in length. In this study, long DNA molecules (~16μm λ-DNA) were used as substrate to study the effects of Integration Host Factor (IHF) binding because our aim focused is on non-specific interactions. Therefore, we used transverse magnetic tweezers instead of vertical magnetic tweezers.

Transverse magnetic tweezers (TMT) setup, as illustrated in Fig. 16A, is designed to pull a single DNA in the focal plane of the objective, making it straightforward to observe the real-time DNA extension dynamics [45, 46]. In my experiment, the two 12-nt sticky ends of 48.5 kb λ-DNA molecules (48,502 bp, New England Biolabs) were labeled using biotin-oligonucleotides using ligation reaction [38] and incubated in a flow channel (as shown in Fig. 17C) which allows for quick and easy changing of solution. The single-DNA tethers are formed between 2.8-μm-diameter streptavidin coated paramagnetic beads (Dynalbeads M-280 Streptavidin, Invitrogen, Singapore) and the edge of a functionalized 0# cover glass (Paul Marienfeld GmbH & Co.KG) through streptavidin-biotin ligand interactions [46]. A permanent magnet is fixed and controlled by micro-manipulator (Fig. 17A - Fig. 17C) to create an adjustable magnetic field around the flow channel. Force was applied to the DNA substrate through the attached paramagnetic bead. A 40X microscope objective is used to image the tethered bead onto a CCD camera (Pike F-032, Allied Vision Technologies, Germany) at ~100 frames per second. A home-written software with LabVIEW (National Instruments, US) was used to track the paramagnetic bead (Fig. 16B). In this setup, we can apply constant force over a wide range from 0.01pN to 200pN. We can also get high spatial and temporal resolution

of 2nm and 500HZ respectively. In the next section, more details of force calibration and single tether determination of this transverse magnetic tweezers will be further explained.

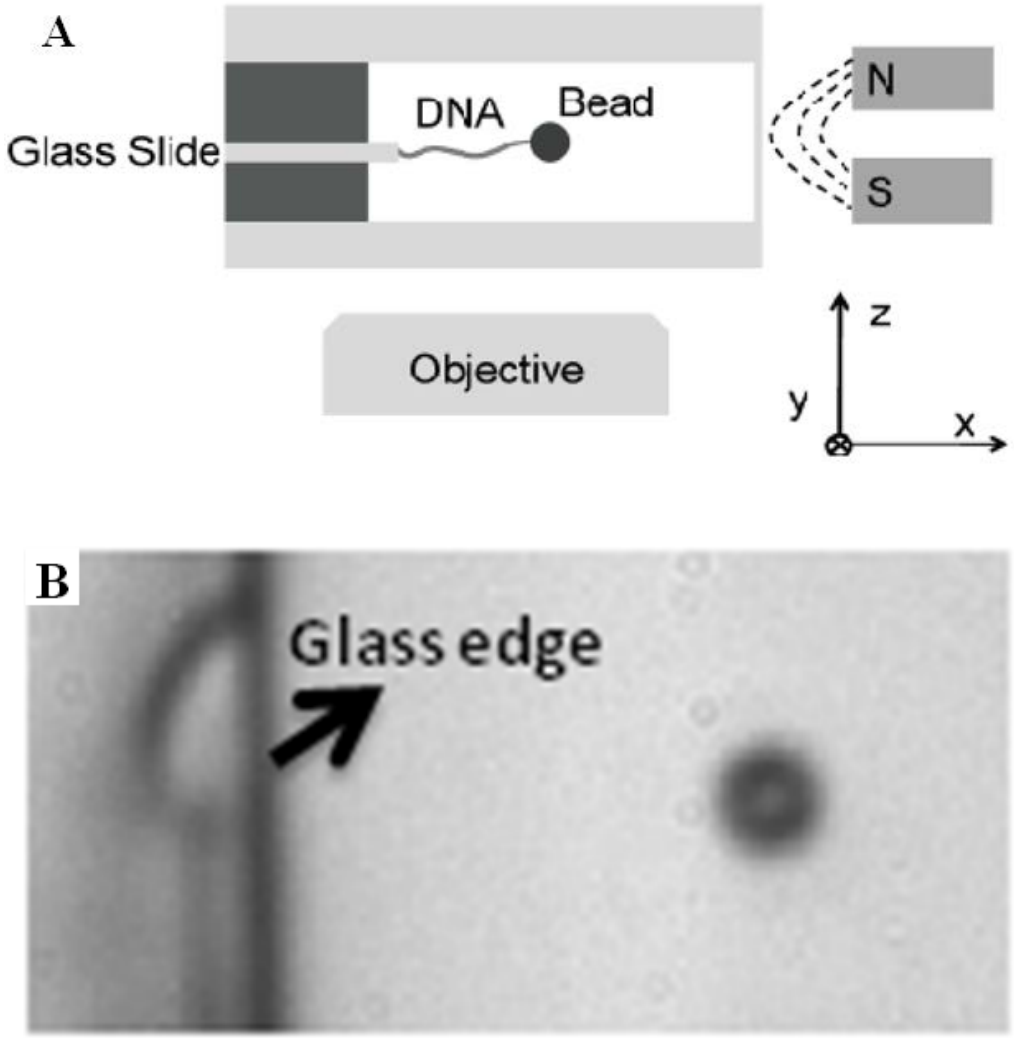

Figure 16. A) Transverse magnetic tweezers setup **B)** The screenshot of the LabVIEW control software during one of the magnetic tweezers experiments.

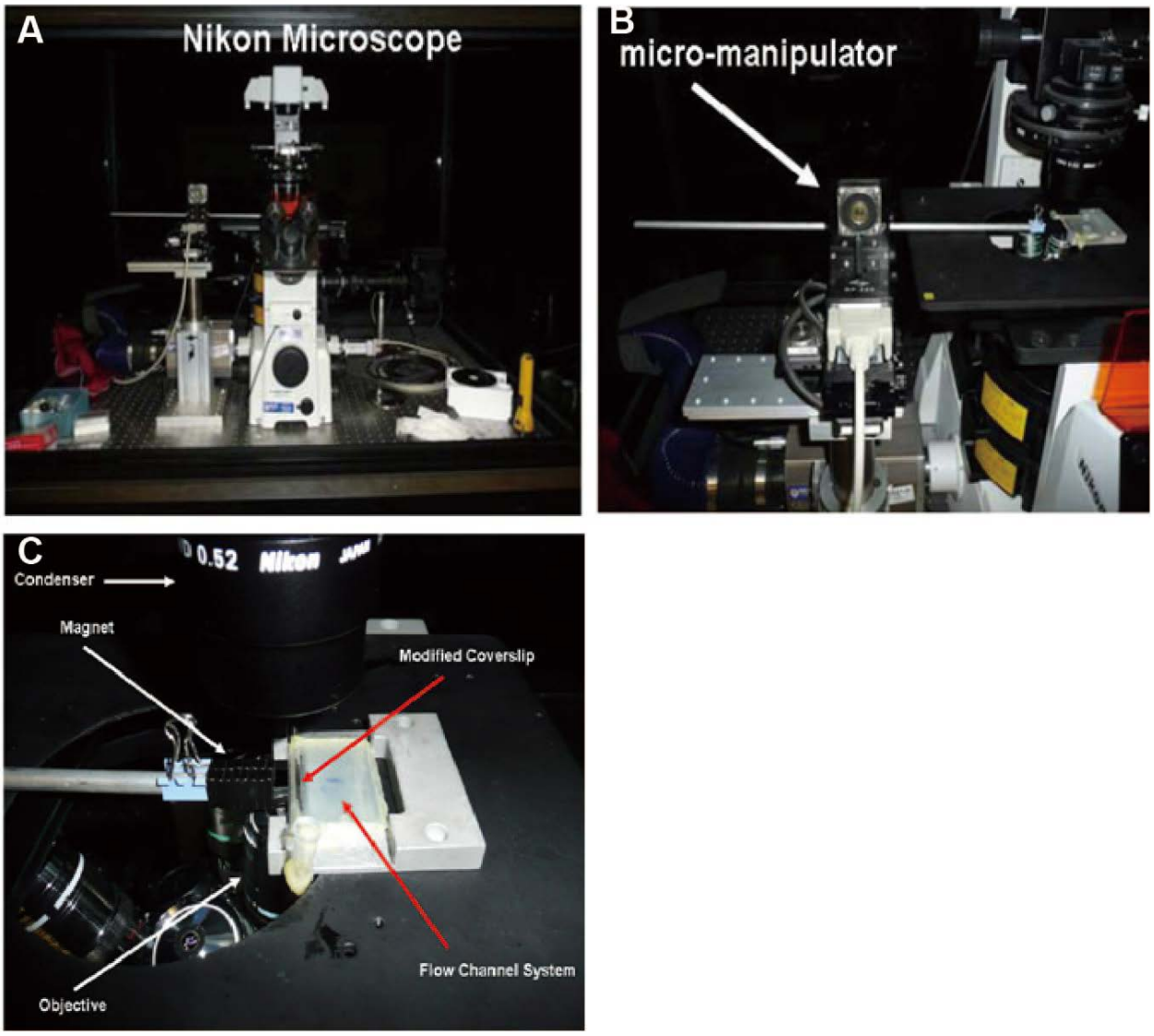

Figure 17. A) Transverse magnetic tweezers set up in my study. **B)** Zoom-in picture of miro-manipulator in this set up. **C)** Zoom-in picture of flow channel and magnets.

2.2.3 DNA EXTENSION MEASUREMENT, FORCE-CALIBRATION AND DETERMINATION OF SINGLE TETHERS

As shown in Fig. 16B, one end of DNA was attached to the functionalized cover glass edge (arrowed dark grey line), and the other end was attached to the paramagnetic bead through streptavidin-biotin ligand interactions. The DNA extension was determined by the distance from the centroid of the magnetic bead to the glass edge. Note that when DNA extension is ~2 μm, the bead is very close to the glass edge, which is also the edge of our observation window. Therefore, we don't let the extension of the DNA go lower than this limit.

Force applied to the DNA substrate through the attached paramagnetic bead was measured by bead thermal fluctuations according to the formula (10), $F = \frac{\mathrm{k_B T}\, z}{\delta y^2}$, which was described in section 2.2.1.

In this single-molecule manipulation, since only the micrometer-sized paramagnetic bead is visible but the attached DNA is not visible, the possibility of multiple DNA tethers may happen, giving inaccurate results. Therefore, before adding any proteins, we must make sure that the attached DNA tether is a single tether. This determination is executed as follows: the force-extension curve of bare DNA molecule was recorded and the persistence length was calculated by fitting the Marko-Siggia formula, $\frac{fA}{\mathrm{k_B T}} = \frac{1}{4}\left(1 - \frac{z}{L}\right)^{-2} - \frac{1}{4} + \frac{z}{L}$, when the force range is from 0.5pN to 10pN. The DNA tether between the glass edge and the paramagnetic bead was identified as a single tether if

the value of its persistence length is about 44 nm~53 nm [46]. After force calibration and single-tether determination, experiments involving proteins can be performed.

2.3 SINGLE-MOLECULE IMAGING BY ATOMIC FORCE MICROSCOPY

2.3.1 PRINCIPLES OF AFM IMAGING TECHNIQUE

In 1986, Binnig, Quate and Gerber invented the first atomic force microscopy (AFM). From that time, AFM has become one of the most powerful tools to measure, image and manipulate matter with nanometer resolution [47-49]. AFM has many advantages over its predecessor, the scanning electron microscopy (SEM). First, it does not require pre-image sample treatment, such as carbon coatings in SEM, i.e. it will not damage or change the samples. Some AFMs even allow liquid environment imaging, which benefits biological studies a lot. Moreover, during the AFM imaging process, tapping mode, which is one of the major imaging modes of AFM, is commonly used to reduce sample damage by touching the sample surface gently and discontinuously. Secondly, the AFM images are three-dimensional while images from SEM are only two-dimensional.

The major components of AFM are a cantilever with a sharp probe, a laser beam deflection system, an electronic PZT scanner and a system control computer, as shown in Fig. 18 and Fig 19. The probe of the cantilever is coated by silicon or silicon nitride

with a radius of nanometers curvature. A laser beam is reflected from the back of the cantilever and onto an array of photodiodes detector. When the probe is brought near to the sample surface, force between the probe and the sample lead to a distortion of the cantilever, which in turn change the direction of the reflective laser beam. This information will be translated into the sample surface three-dimensional images through the photodiode detector and the control system.

There are two major modes in atomic force microscopy, which are contact mode and tapping mode, according to whether the probe continuously contacts with the surface.

In contact mode, the probe is brought in contact with the sample surface. The cantilever is deflected by the force between the probe and the sample. This deflection is used as a feedback signal to allow the AFM to create of images of the sample. However, because the probe has physical contact with sample all the time, it may damage fragile or soft samples or even stick to sample surface, a problem for most biological specimens.

In tapping mode, the cantilever is driven to oscillate up and down at its resonance frequency. The probe is close enough to the sample to make short-range forces detectable while far enough to avoid the tip damaging or sticking to the sample. It is very suitable for biological samples imaging because the conformation of the sample molecules can remain unchanged for hours with good operating parameters.

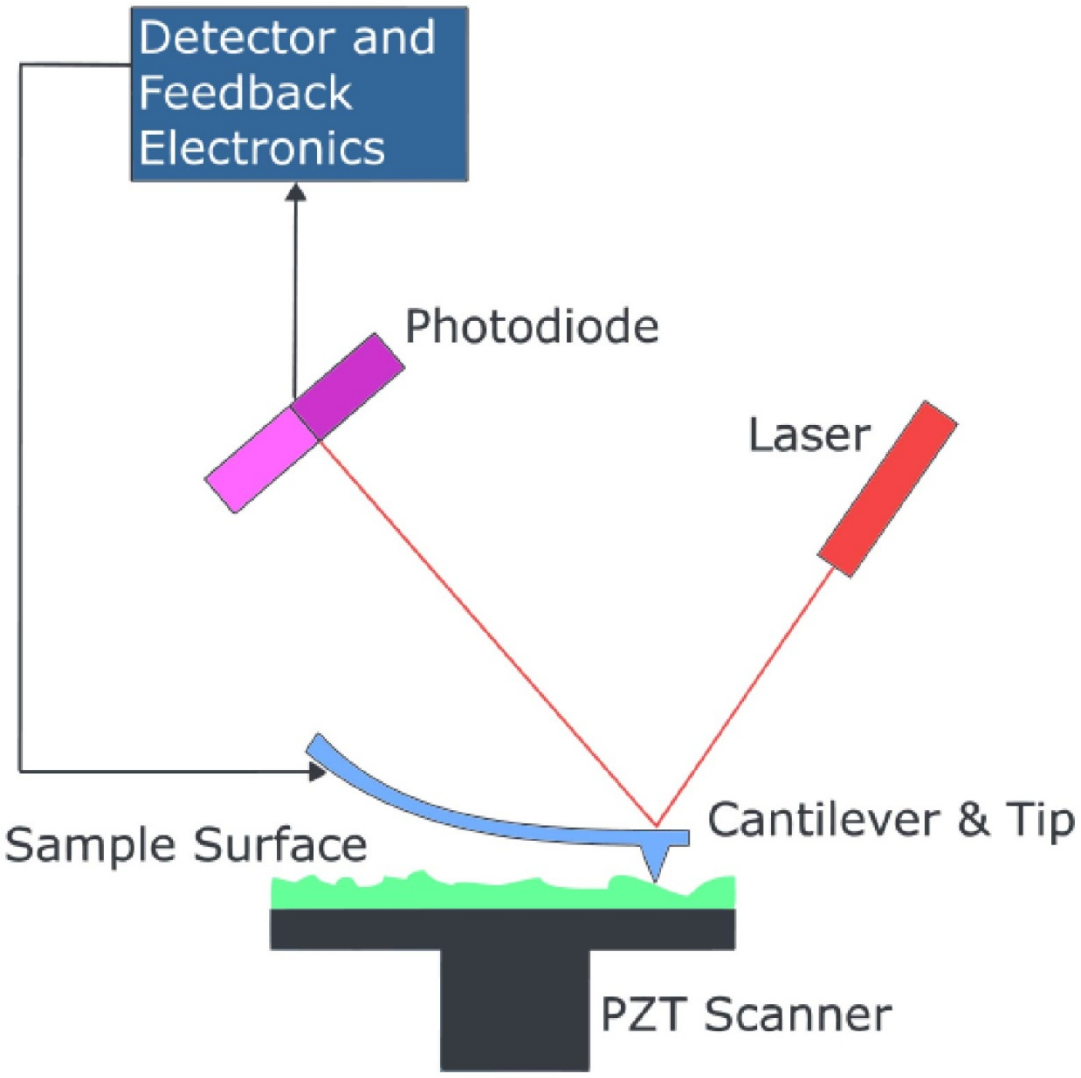

Figure 18. Schematic diagram of Atomic Force Microscopy (from wikipedia)

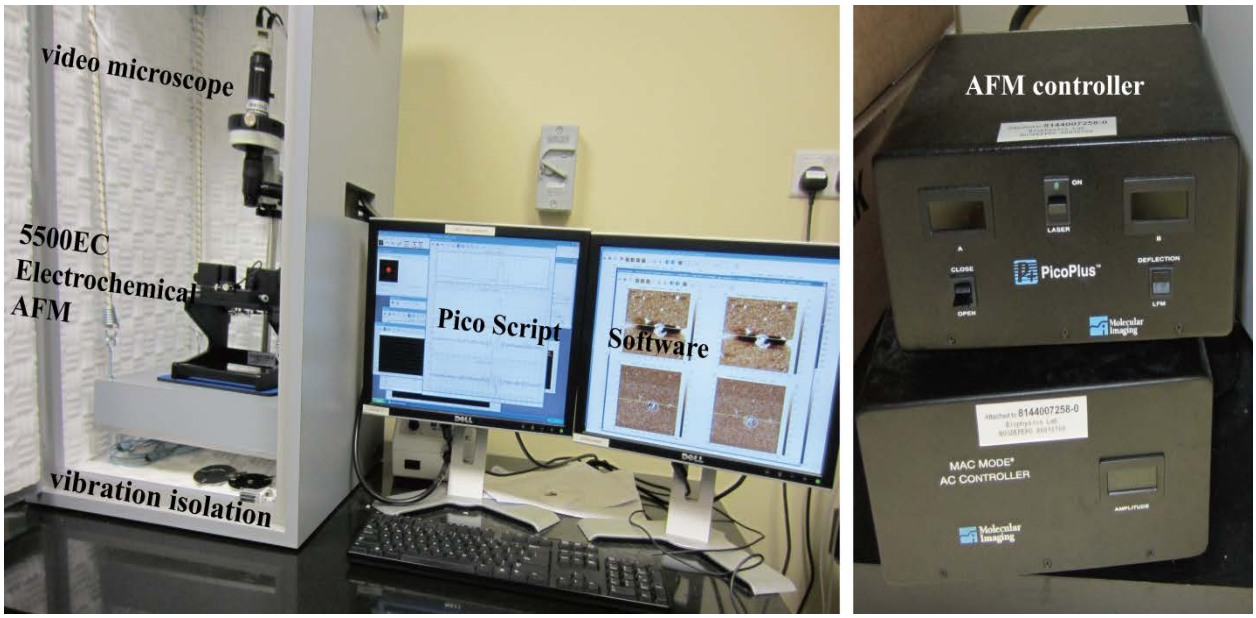

Figure 19. Molecular Imaging 5500 AFM (Molecular Imaging, Agilent Technologies) set-up in my lab. The left is the core part of AFM, the middle is the software and sceen, and the right part is the AFM controller.

2.3.2 FUNCTIONALIZATION OF MICA SURFACE FOR IMAGING EXPERIMENTS

As described in the last section, atomic force microscopy with tapping mode provides a powerful means to image biological structures. Plenty of techniques for sample preparation have been used to optimize image effect and avoid sample damage. Some of these techniques, which were used in my study, are described here, including fresh-mica, AP-mica and Glu-mica.

AFM samples should be immobilized on a rigid support. The size of biological specimens such as DNA, proteins and DNA-protein complex is usually in the order of nanometers. Accordingly, these biological structures need to be bound to a very flat substrate. Mica is a very common substrate because it is atomically flat, easy to cut to preferred size and relatively cheap.

First, some DNAs or proteins are prepared by incubating them onto fresh cleaved mica (Fresh-mica). However, one problem arises. When mica contacts water, it is negatively charged. DNAs or some proteins in solution are also negatively charged. Thus DNAs or proteins are repelled away from the fresh-mica surface by electrostatic interaction, and cannot be incubated on the fresh-mica. Divalent cations, such as Ni^{2+} or Mg^{2+}, are added to the solution to serve as a counter ion on the negatively charged DNA or protein backbone and also provide additional charge to bind to the fresh-mica [50].

Although divalent ions make a bridge between fresh-mica surface and DNA or protein molecules, they may also cause unexpected condensation to DNA or protein by neutralizing the intrinsic charges of the molecules. Moreover, adding divalent ions, such as magnesium, which has great influence on the DNA-protein interactions, may cause fake AFM images of the protein/DNA complex. One mica functionalization based on silanizing fresh mica surface with 3-aminopropyltriethoxysilane (APTES) [51] is developed to avoid adding divalent ions. The reaction is shown in Fig. 20. In AP-mica, the amino groups of APTES are covalently bound to the fresh mica, which makes the modified mica surface is positively charged to hold DNAs or some proteins (negatively

charged) tightly. The amount of APTES added is very crucial to the imaging results. It is usually highly diluted at the concentration of 0.1% (see section 2.5.2 for details) because high concentration APTES solution cause large surface roughness which makes nanometer sized DNA or protein indistinguishable. Another problem of AP-mica is that positively charged AP-mica might influence the morphology of DNA-protein complex by repelling the proteins away from DNAs electrostatically.

Glu-mica is created to solve the DNA-protein AFM imaging issues by simply adding another glutaraldehyde layer to AP-mica surface [51], as illustrated in Fig. 20. This method can be utilized to covalently immobilize various proteins, DNA-protein complexes and other molecules with free lysine residues to mica surface. Since Glu-mica can provide stable and reliable images of DNA-protein composites, it was used in this study to provide vivid three-dimensional pictures of DNA-IHF interactions [51, 52]. The protocol of Glu-mica modification is introduced in section 2.5.2.

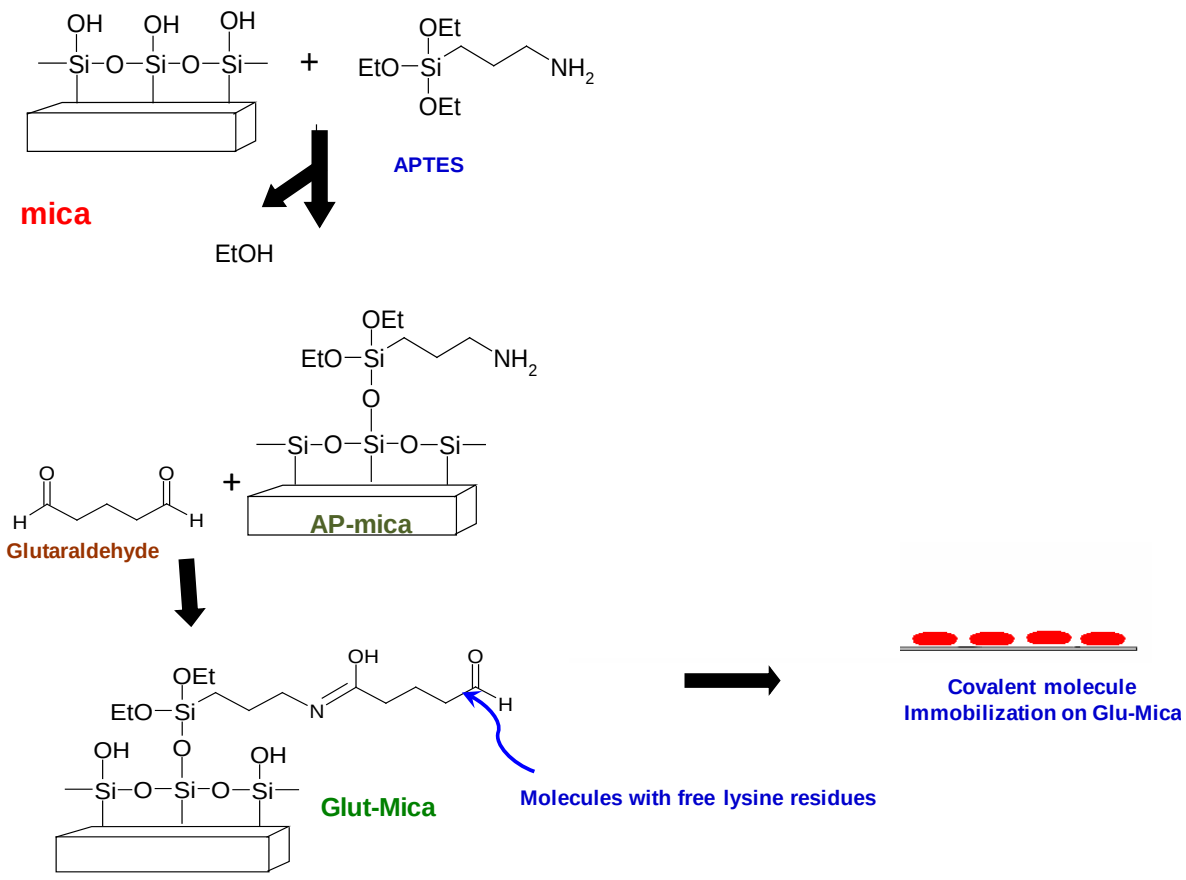

Figure 20. Schematic diagram of mica modification process, including AP-mica and Glu-mica.(Figure produced by modifying the protocol of CHROMATIN 1.0 by Travis Johnson in Agilent Technologies).

2.4 EXPRESSION, PURIFICATION AND CONCENTRATION MEASUREMENT OF INTEGRATION HOST FACTOR

Purified IHF proteins used in this study are provided by our collaborator Peter Droge from Nanyang Technological University, Singapore. The protein expression and purification were done in Peter's lab, which are described in his published paper [53].

IHF protein molecular weight and purity were double-checked in our lab by gel electrophoresis. Gel Electrophoresis is the study of molecular mobility in an electric field. Mediums acrylamide and agarose are generally used for proteins and DNA studies respectively. In this study, we focus on protein electrophoresis by SDS-PAGE to check the IHF molecular weight and purity.

SDS-PAGE treats proteins under denaturating conditions, meaning that secondary, tertiary and quaternary structures are disrupted to produce a linear polypeptide chain coated with negatively charged SDS molecules. Then the protein migrates only depending on its size (molecular weight) because the number of SDS molecule bound to a protein is proportional to the number of amino acids. As shown in Fig. 21, it is the result of the SDS-PAGE of the purified integration host factor used in my study. According to the molecular weight markers, two lines (not very clearly due to similar size), corresponding to α and β subunits of IHF, weighted about 10KDa of each, are observed. This result is consistent with the structure of IHF protein.

IHF protein concentration was measured by Nanodrop ND1000 (Wilmington, U.S.A). Nanodrop ND100 calculates protein concentration by detecting purified proteins exhibiting absorbance at 280nm in the resolution of 0.1mg/ml.

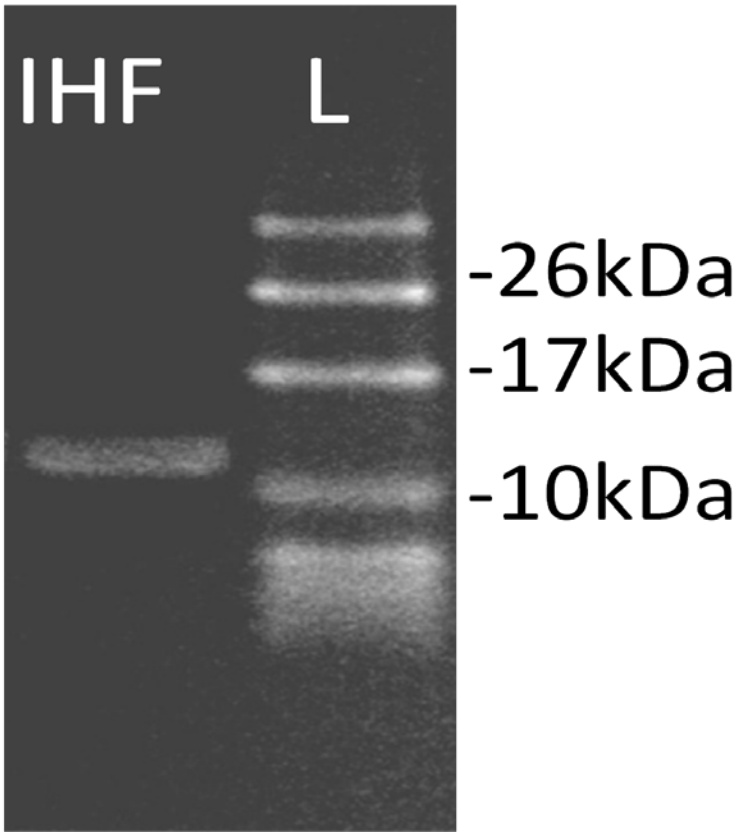

Figure 21. Purified IHF (5 ug) was analyzed by (18%) SDS-PAGE, together with molecular weight markers (L).

2.5 EXPERIMENT PROCEDURES AND DNA CONSTRUCTS

2.5.1 MAGNETIC TWEEZERS EXPERIMENTS

Biotin labeled λ-DNA (48,502 bp, New England Biolabs) molecules at the two DNA ends of the opposite DNA strands, named as b-λ-b DNA, were used for magnetic tweezers experiments. First, the b-λ-b DNAs in 1xPBS buffer were incubated for 20 minutes in the

flow-channel to fix one end to the streptavidin-coated glass edge. Then 2.8μm-diameter paramagnetic beads (Dynalbeads M-280, Invitrogen, Singapore) in 1xPBS buffer solution were added into the channel to attach the other end of b-λ-b DNA by streptavidin-biotin linkage. After washing away the unattached paramagnetic beads by the reaction buffer, this flow channel was ready for use in transverse magnetic tweezers experiment. The tweezers are capable of stretching a single DNA in the focal plane of objective; therefore DNA structure transition dynamics can be studied directly. Before adding proteins, the force-extension curve of dsDNA was recorded and the persistence length was calculated by fitting the Marko-Siggia formula to identify whether the tether studied was a single DNA (please see section 2.2.2 and 2.2.3 for more details). After single-tether confirmation, proteins with different concentrations in reaction buffer were flowed into the channel and the DNA extension changes under different forces were recorded in real time. All experiments were conducted at room temperature except illustrated specially.

2.5.2 AFM IMAGING EXPERIMENTS

ΦX174 RF I DNAs, which is circular and 5,386bp, were purchased from New England Biolabs. These DNAs were digested with restriction enzyme PstI (New England Biolabs), which has one cutting site along circular ΦX174 RF I DNA. After that, ΦX174-PstI DNAs, which became linear, were used in the AFM experiments.

The mica was prepared by depositing 0.1 % APTES solution on a 0.5 cm x 0.5 cm piece of mica for 10 minutes. The mica was then rinsed with deionised water, dried with nitrogen gas before incubating in a desiccator for at least two hours. Then 1 % glutaraldehyde solution was deposited for 10 minutes and the mica was washed and dried as before. The Glu-mica is either used directly or stored in a desiccator (< 12hours) for future use.

The solution of 0.2 ng/µl linearized ΦX174 DNA with an appropriate concentration of IHF was mixed and incubated for 20 minutes. The solution was then deposited on the mica for 20 minutes. After that the mica was washed with 3 millilitres of deionised water and then dried with nitrogen gas slightly.

AFM imaging was performed by AC-mode in air with 60% humidity using Molecular Imaging 5500 AFM (Molecular Imaging, Agilent Technologies). The AFM probe used in all the measurements is silicon AFM probe (Taq300, Budget Sensors).

CHAPTER 3: NON-SPECIFIC BINDING OF INTEGRATION HOST FACTOR REGULATES CHROMATIN ORGANIZATION

3.1 ABSTRACT

As described in the previous chapters, the integration host factor (IHF) protein is an abundant nucleoid protein that is involved in phage λ site-specific recombination and gene regulation in *E.coli*. Introduction of a sharp DNA bend at binding sites specific for IHF is thought to be critical for these functions. Interestingly, the intra-cellular concentration of IHF is larger than the concentration needed for its site-specific functions, suggesting that non-specific binding of IHF to DNA may play a role in the physical organization of bacterial chromatin. However, it is unclear how non-specific binding of IHF contributes to DNA organization.

Using a combination of single-DNA manipulation and atomic force microscopy imaging methods, we show that distinct modes of non-specific binding of IHF to DNA result in complex DNA conformations. Changes in KCl concentration, IHF concentration, and force can change the sharpness of DNA bending. In addition, IHF can crosslink DNA into a highly compact meshwork structure that is observed in the presence of magnesium at low concentration of monovalent ions, and high IHF-DNA stoichiometries. Our findings provide important insights how IHF contributes to bacterial chromatin organization, gene regulation, and biofilm formation.

3.2 KCL CONCENTRATION AFFECTS THE INFLUENCE OF IHF ON THE FORCE RESPONSE OF SINGLE DNA

We first used transverse magnetic tweezers to study changes in the force-response of single λ-DNA (48,502 bp) in response to changes in IHF and KCl concentrations at 20 ^{o}C and pH 7.4 (Fig. 22). For IHF concentrations ranging from 0–1,250 nM, the force-extension curves were recorded in 200 mM KCl (Fig. 22A). To determine if IHF binding reached a steady or equilibrium state, the data were recorded using a forward force scan, during which the force was sequentially decreased from higher to lower values, followed by a reversed force scan by increasing the force through the same set of force values to determine if hysteresis exists. At each force, data was recorded for 30 s, and the data obtained in the last 5 s was used to calculate the extension. No hysteresis was observed in the reverse force scans, suggesting that IHF-DNA interactions reach equilibrium within the experimental time scale. DNA extension monotonically decreases as IHF concentration increases. At saturation binding concentration of IHF (> 500 nM), IHF binding weakly reduces DNA extension. At 1,250 nM IHF [54], the DNA becomes ~20% shorter than naked DNA. Overall, our data are consistent with results of others obtained under the same KCl concentration (Fig. 23) [54].

To understand how IHF-DNA interactions depend on the KCl concentration, we varied the KCl concentration. We found that DNA is significantly less extended at 100 mM KCl than at 200 mM KCl (Fig. 22A and B). Extension at 50 nM IHF in 100 mM KCl is comparable that obtained at 1,250 nM IHF in 200 mM KCl, where saturation binding is

achieved (Fig. 22B). If IHF induces equal DNA bending at 200 mM KCl and 100 mM KCl, saturation binding should occur at 100 mM KCl and ~50 nM IHF. However, when IHF concentration is increased above 50 nM, DNA extension decreases. This suggests that IHF reduces DNA extension through different mechanisms at 100 mM KCl and 200 mM KCl. Because no hysteresis was observed in the reverse force-extension curve, this increased DNA bending is not likely due to global DNA condensation caused by mechanisms such as DNA looping or DNA bridging. Rather, it may be due to DNA bending at a sharper angle than occurs at 200 mM KCl. In addition, DNA extension was non-monotonically dependent on IHF concentration at 100 mM KCl. When IHF concentration was increased from 250 nM to 1,250 nM in 100 mM KCl, DNA extension increased, rather than decreasing monotonically.

To understand how KCl concentration affects the DNA binding properties of IHF, we repeated this experiment at a KCl concentration of 50 mM. Similar non-monotonic dependence of DNA bending on IHF concentration was observed at 50 mM KCl (Fig. 22C), where the maximal bending occurs at ~50 nM IHF. Note in 50 mM KCl, slow hysteretic DNA compaction occurs, and the level of hysteresis increases as IHF concentration increases. The existence of hysteresis indicates that, in addition to DNA bending, there is another DNA folding mechanism with a slower kinetics. It indicates either an even sharper DNA bending with a slower kinetics or DNA condensation into higher order complex structures by IHF in 50 mM KCl. In order to separate the contribution from DNA folding from the slower DNA condensation, it will be good to minimize the interference from DNA condensation by reducing the duration when DNA is held at small force values. This is achieved by the quick force-jumping method

explained below. In the force-jumping experiments, the DNA is held at > 10 pN to prevent DNA folding during the introduction of IHF solution into the reaction channel. Then, the force is jumped to a lower value and the DNA extension is recorded by holding the DNA for only ~ 10 s. Then the force is jumped back to the high force to ensure the DNA extension returned to the original value of the naked DNA. Repeating this process for a series of other lower force values, the force-extension curve of DNA can be obtained. In such experimental procedure, slow DNA folding occurring at a lower force value will not accumulate to the next lower force data point; therefore, the interference from slow DNA folding is reduced. Using the force-jumping method, the force extension curve of another λ-DNA measured in 50 mM KCl (Fig. 22D) is very similar to Fig. 22B obtained in 100 mM KCl, which again suggests a sharper DNA bending than in 200 mM KCl and a non-monotonic dependence of the DNA extension reduction on the concentration of IHF.

The non-monotonic dependence of the DNA extension on IHF concentration suggests that the level of DNA bending is mediated by IHF concentration and that sharp DNA bending is not favored at high IHF concentrations. To quantify this non-monotonic dependence, the DNA extensions recorded at 200 mM KCl (Fig. 22A), 100 mM KCl (Fig. 22B), and 50 mM KCl (Fig. 22D) are plotted as functions of IHF concentration (Fig. 22E). At 200 mM KCl, DNA extension monotonically decreases as IHF concentration increases, whereas at 100 mM and 50 mM KCl, there appears to be a critical IHF concentration, below which DNA extension monotonically decreases as IHF concentration increases and above which DNA extension monotonically increases as

IHF concentration increases.

These results reveal non-specific interactions between IHF and DNA. Binding of IHF to DNA, inducing a fixed bending angle, cannot explain these results. The existence of at least two DNA bending states that depend on both KCl concentration and IHF concentration would explain the differential force-response of the DNA-IHF complex to these factors. In addition, the hysteresis observed in 50 mM KCl suggests that a possible slower DNA condensation may also exist at low KCl concentration. These hypothesized mechanisms will be investigated in details in subsequent sections.

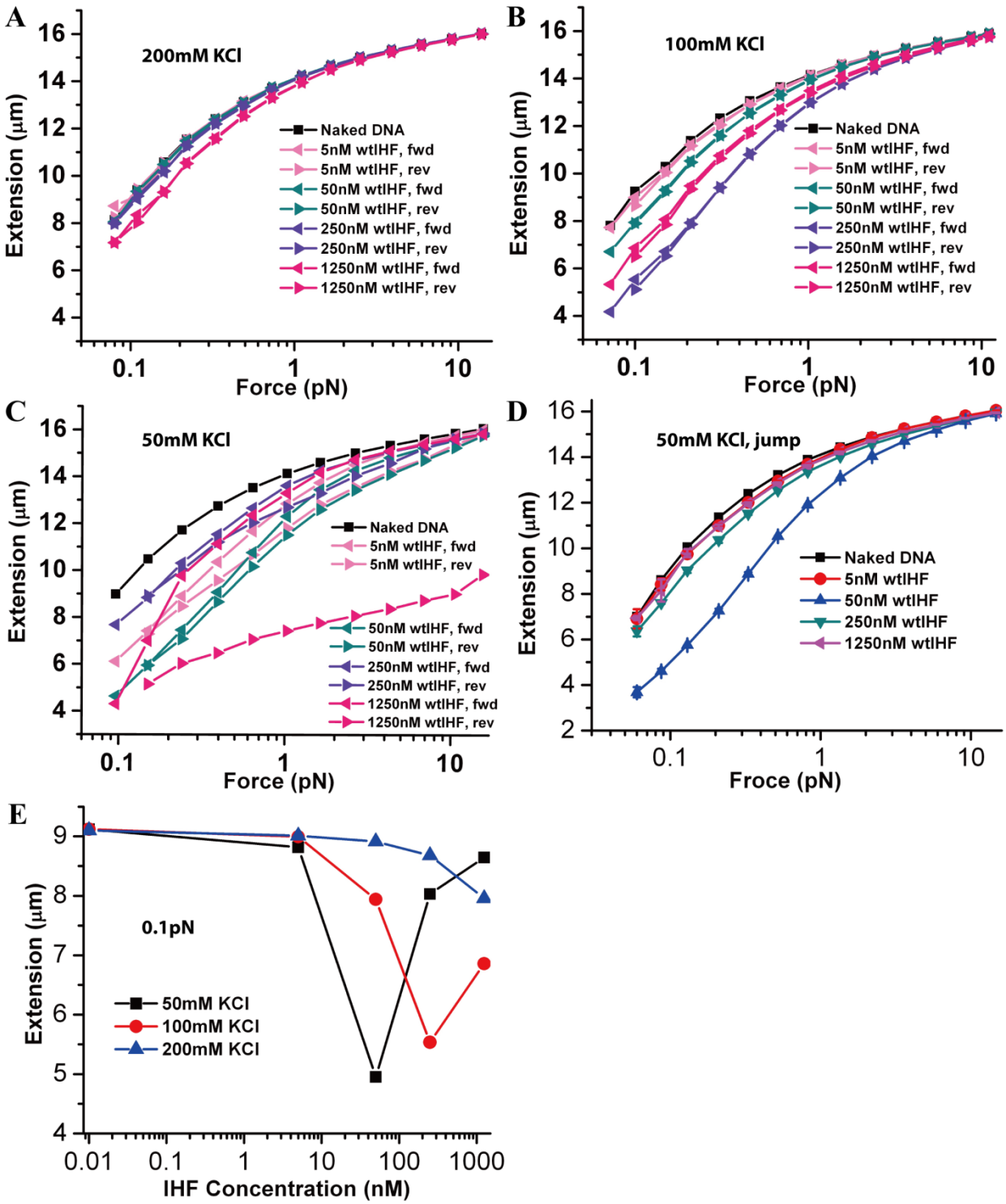

Figure 22. Effects of IHF on the force response of 48,502 bp λ-DNA at varying concentrations of KCl and pH 7.4. **A)** Forward and reverse force-extension curves of

DNA at the indicated concentrations of IHF in 200mM KCl. At saturation (1,250 nM IHF), DNA extension is only slightly reduced, compared to the naked DNA at small force region, implying weak DNA bending by IHF. No hysteresis was observed in the reverse curve, suggesting that IHF-DNA interaction reached a steady state under these conditions. **B)** In 100 mM KCl, a non-monotonic relation between the DNA extension and IHF concentration is observed. At non-saturated ~250 nM IHF, maximal DNA extension reduction occurs, which is significantly greater than in 200 mM KCl when saturation binding occurs at 1,250 nM IHF. No hysteresis was observed in the reverse curve, suggesting that IHF-DNA interaction reaches a steady state over the experimental time scale. **C)** In 50 mM KCl, a similar non-monotonic relation between the DNA extension and IHF concentration is observed, except that the maximal DNA extension reduction occurs at a smaller IHF concentration (~50 nM). A difference from 100 mM KCl is that hysteresis was observed in the reverse curves, and becomes larger at higher IHF concentrations. This suggests that in addition to DNA bending, a slower DNA condensation may also contribute to the DNA extension reduction. **D)** Re-measuring the force-extension curves in 50 mM KCl by a quick force jumping method (see details in main text) to only probe the contribution by DNA bending to DNA extension change. The force-extension curves obtained in this way again demonstrates the non-monotonic relation between the DNA extension and IHF concentration. **E)** DNA extension as a function of the IHF concentration at ~ 0.1 pN in different KCL concentrations. Data at 0.1 pN were obtained from the force-extension curves at corresponding KCl concentrations in Fig. 22A-B&D by linear interpolation using two nearest neighboring data points adjacent to 0.1 pN.

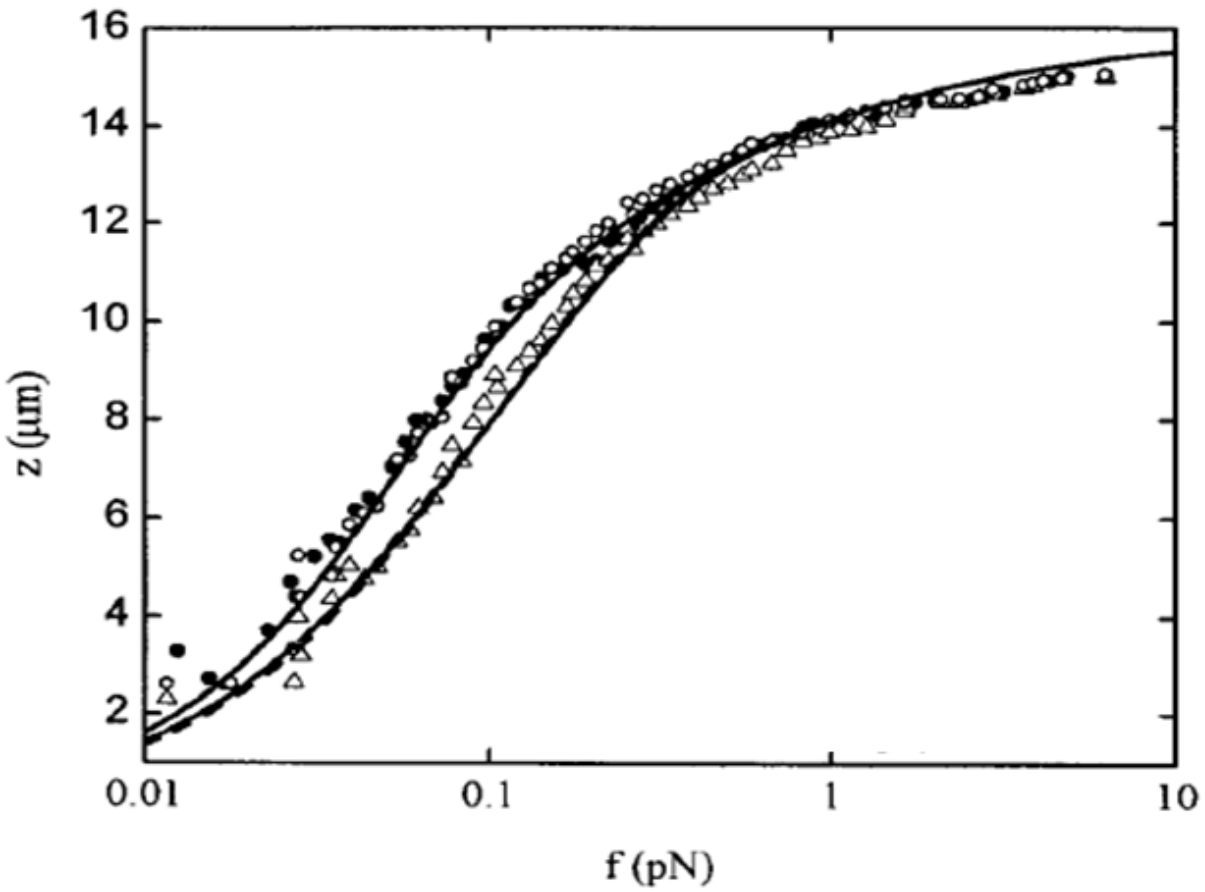

Figure 23. Previous study of the force-extension curves of 48,502 bp λ-DNA in 200 mM KCl solution at different concentrations of IHF: 0 nM IHF (full circles), 1250 nM IHF (empty triangles) [54]. (For the purpose to compare with my result, according to Copyright and License policy of PNAS).

3.3 KCL CONCENTRATION MEDIATES SWITCH BETWEEN WEAK AND SHARP BENDING OF IHF-DNA COMPLEX

At an IHF concentration of saturated binding (e.g. 1,250 nM), DNA is more extended in 200 mM KCl than the shortest DNA extension at 50 mM or 100 mM KCl (Fig. 22E). To

determine if decreasing the KCl concentration induces sharper DNA bending, a DNA tether was incubated at varying concentrations of IHF in 200 mM KCl and then at 50 mM KCl without free IHF proteins. If most of the IHF bound to the DNA in 200 mM KCl do not dissociate during exchanging buffer solution, one should expect to see the response of IHF-DNA complex to the change in KCl concentration which is not impacted by free IHF in solution.

At 200 mM KCl and the unsaturated IHF concentration of 50 nM IHF, the force-extension curve almost overlaps with the reference curve obtained from naked DNA before IHF was added (Fig. 24). However, at 50 mM KCl in the absence of IHF, DNA extension was reduced slightly by ~ 600 nm at ~ 0.08 pN (Fig. 24). This decrease in DNA extension was not caused by effects of salt on the elasticity of naked DNA, as the force-response of DNA is almost identical in KCl concentrations ranging from 50–200 mM (Fig.25). Repeating this experiment at IHF concentration of 250 nM or the saturated concentration of 1,250 nM, we obtained similar results but with greater DNA extension reduction. These findings support the existence of at least two distinct DNA bending modes of the IHF-DNA complex. Because there was no free IHF in the 50 mM KCl solution, the reduced extension that occurred after changing the buffer should have resulted from the response of DNA-bound IHF to the change in KCl concentration.

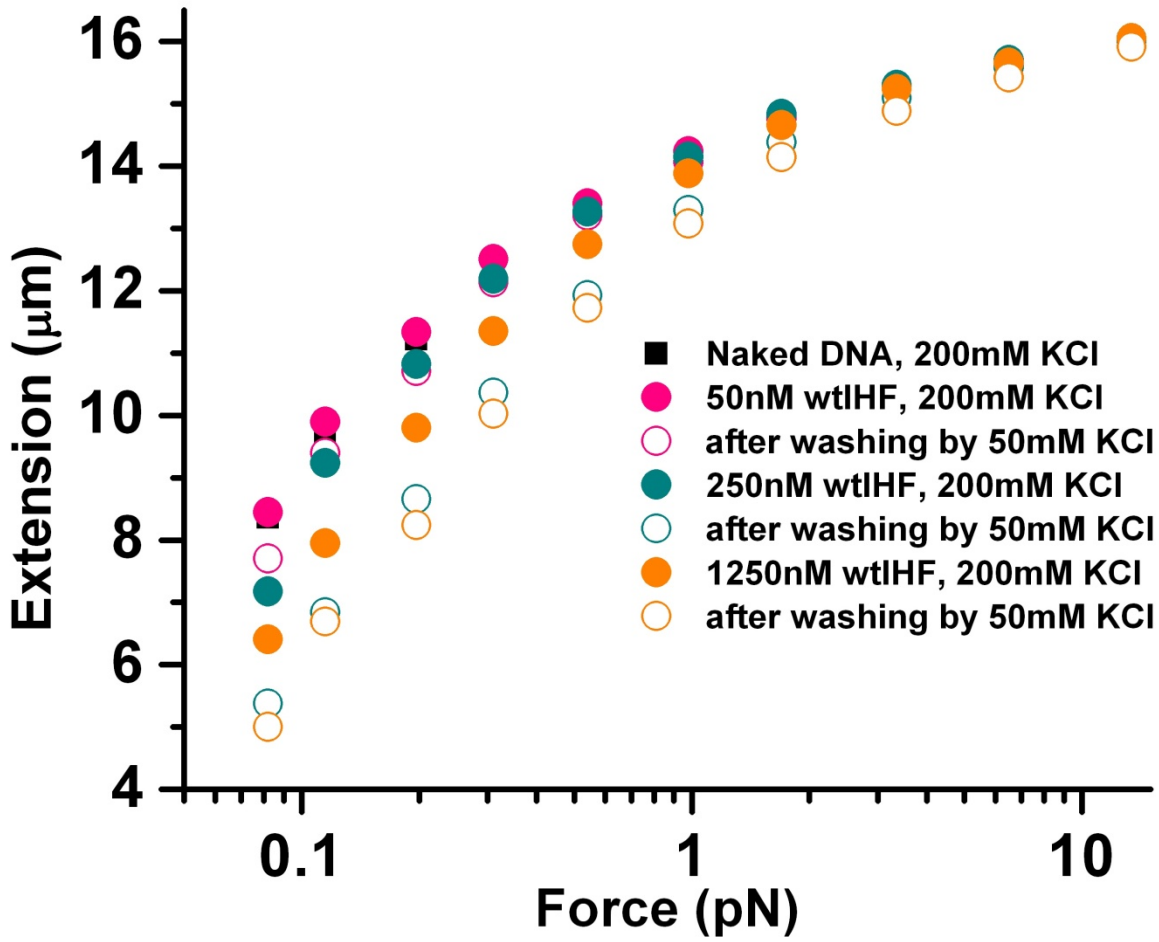

Figure 24. Decreasing KCl concentration, from 200 mM KCl to 50 mM KCl, drives a switch from a weaker DNA bending conformation to a sharper DNA bending conformation. Filled circles represent force-extension curves of DNA incubated in 200 mM KCl and the indicated concentration of IHF. Open circles represent force-extension curves of DNA after lowering the KCl concentration to 50 mM and removing IHF. The shift of the force-extension curves after lowering the KCl concentration and removing the IHF molecules that were pre-bound to DNA at 200 mM KCl indicates the subsequent change in DNA extension.

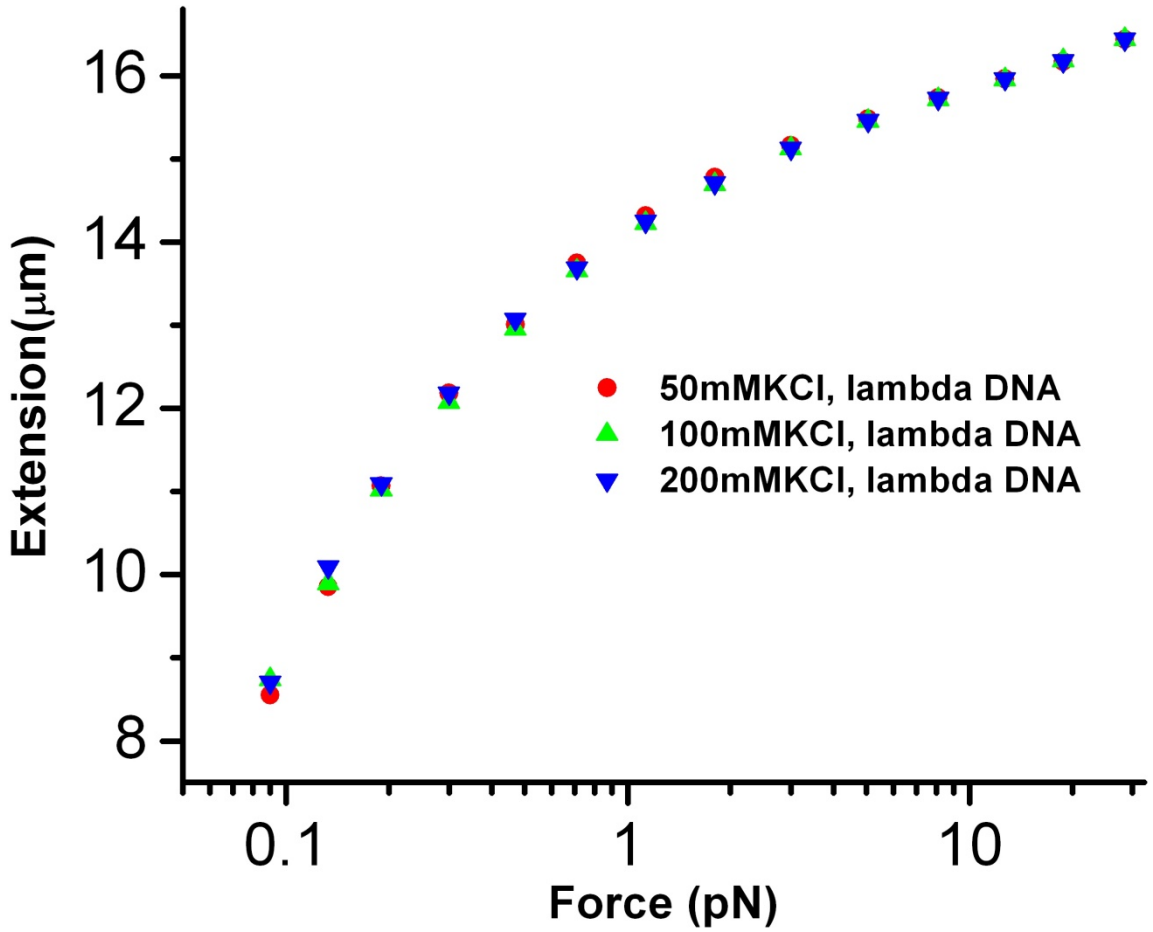

Figure 25. Force-extension curves of λ-DNA in 50 – 200 mM KCl and pH 7.4 (10 mM Tris). It shows that the force-response of DNA is almost identical in various KCl concentrations.

3.4 THE SHARPER DNA BENDING IS INHIBITED AT HIGH IHF CONCENTRATION

A surprising observation is the non-monotonic relationship between the DNA extension and the concentration of IHF observed in 100 mM and 50 mM KCl, where sharper DNA

bending can occur (Fig. 22B-D). In these KCl concentrations, there exists a non-saturated critical IHF concentration (~250 nM IHF in 100 mM KCl and ~50 nM IHF in 50 mM KCl), at which the DNA extension reduction is maximized (Fig. 22 E). This contrasts with in the case of in 200 mM KCl where only the weaker DNA bending is allowed, and where the extension monotonically decreases as IHF concentration increases (Fig. 22A and Fig. 22E).

Such non-monotonic behavior suggests that, in low KCl concentration where the sharper DNA bending is allowed, the sharper DNA bending will be inhibited at high IHF concentration. Otherwise, one would expect that DNA extension monotonically decreases as IHF concentration increases till saturation. Although the mechanism of this IHF concentration dependent transition is not clear, a possibility is that, at high IHF concentration, an IHF occupies less DNA by adopting the less bending conformation to provide room to accommodate more IHF proteins. Furthermore, such overcrowded IHF on DNA may also restrict the level of DNA bending due to expulsive interaction between neighboring IHF proteins when DNA bends. Discussion of this hypothesis will be elaborated in the discussion chapter.

3.5 IHF INDUCES MORE COMPACT DNA CONFORMATIONS AT LOW KCL CONCENTRATION

Although hysteresis did not occur at 100 mM KCl (Fig. 22B), it occurred significantly at 50 mM KCl, and increased with the IHF concentration (Fig. 22C). Hysteresis was

moderate at 50–250 nM IHF (Fig. 22C), but high at 1,250 nM IHF (Fig. 22C). The DNA could not be unfolded to its original extension in the reverse force scan (Fig. 22C). This hysteresis indicates that, in addition to bending, there is another DNA folding mechanism with slower kinetics.

In order to obtain more information of the DNA organization by IHF at different KCl concentrations, we performed AFM imaging experiments on a glutaraldehyde-coated mica surface that is particularly useful for imaging DNA-protein complexes [51, 52]. As the glutaraldehyde molecules are covalently bound to the surface, they do not diffuse into the solution and therefore do not non-specifically crosslink proteins or DNA-protein complexes. Such surface has been shown less perturbing the stability of DNA-protein interactions and is friendly to DNA-protein complex imaging. At 50 mM KCl, naked linear dsDNA (Φx 174, 5,386 bp), which does not contain any consensus IHF sites, assumed an extended random coiled conformation (Fig. 26A). In contrast, addition of 50–250 nM IHF induced more compact DNA conformations (Fig. 26B-D). However, in 50 mM KCl and 1,250 nM IHF, the DNA conformations became significantly more extended than in 50& 250 nM IHF. Similar compact DNA conformation was also observed at 100 mM KCl (Fig. 26 E-F), where sharp DNA bending is also prevalent. In contrast, DNA was weakly bent in single-DNA stretching experiments at 200 mM KCl, and condensation was not observed even at the saturation concentration of 1,250 nM IHF (Fig. 27).

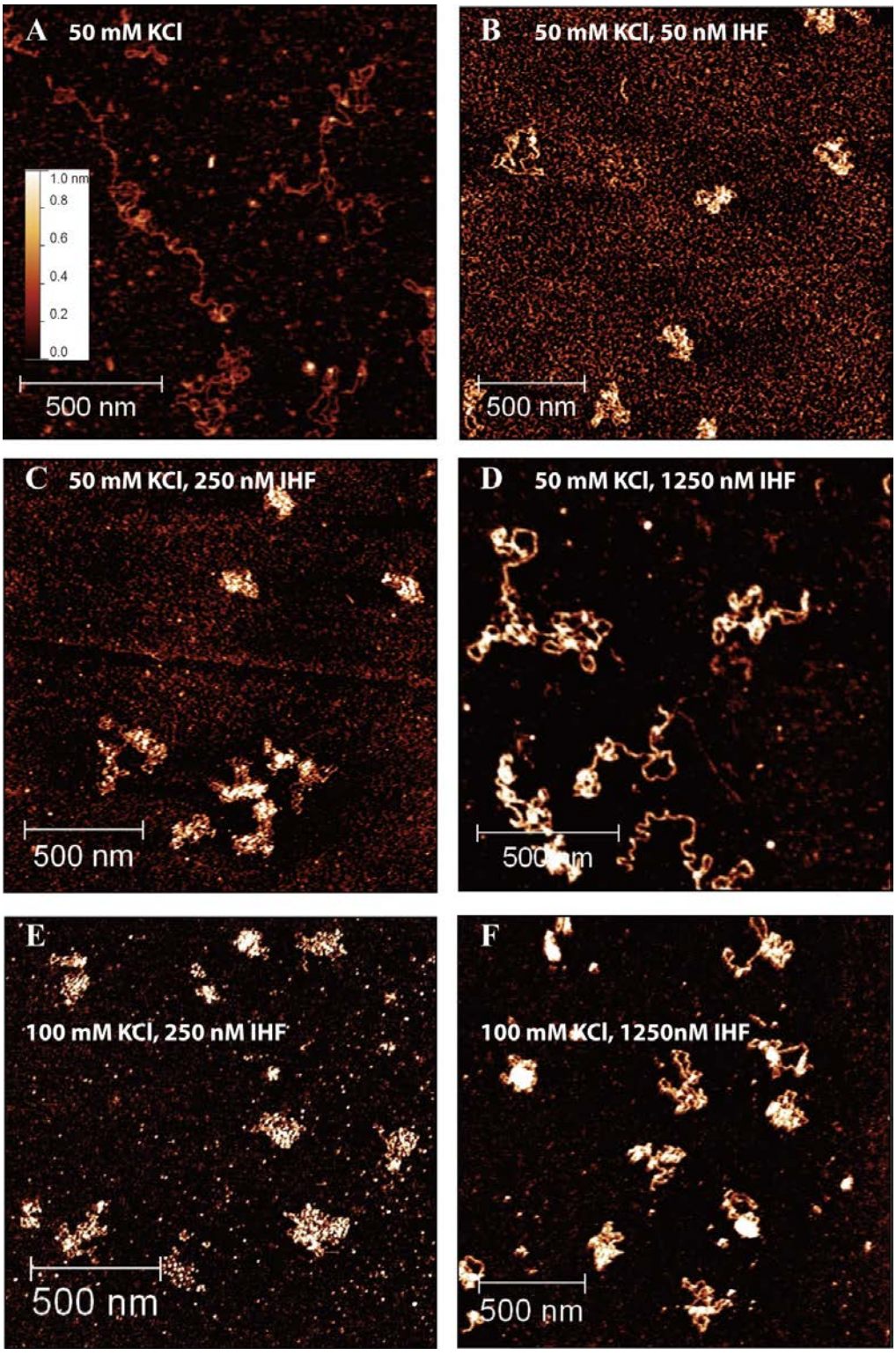

Figure 26. Atomic force microscopy images of linearized double-stranded Φx174 DNA (5,386 bp) incubated with varying concentrations of IHF. **A)** Naked DNA that was not

incubated with IHF in 50 mM KCl as a control. **B)** DNA molecules, incubated with 50 nM IHF in 50 mM KCl. **C)** DNA molecules, incubated with 250 nM IHF in 50mM KCl, show similar compact DNA conformations as Fig. 26B. **D)** DNA molecules, incubated with 1,250 nM IHF in 50mM KCl. Although DNA condensation still occurs, the DNA conformations are more extended compared to those in 50 nM (B) and 250 nM IHF (C) concentrations. This more extended conformation may be caused by IHF overcrowding on DNA in low KCl and high IHF concentrations suggested in Fig. 22 B-E. **E)** DNA molecules, incubated with 250 nM IHF in 100 mM KCl, show compact DNA conformations. **F)** DNA molecules incubated with 1,250 nM IHF in 100 mM KCl, also show compact DNA conformations.

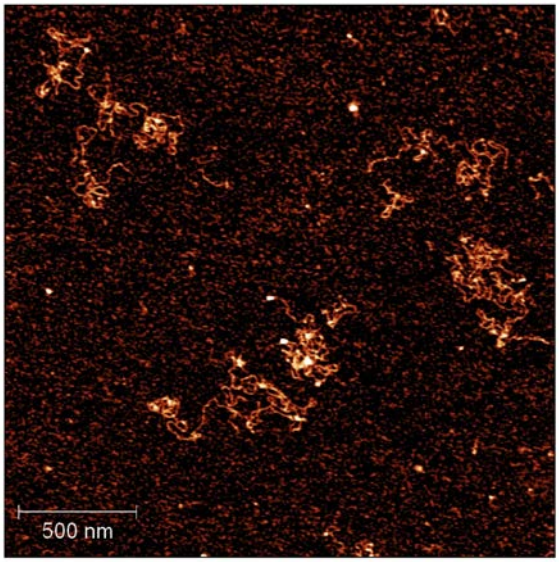

Figure 27. Atomic force microscopy image of linearized double-stranded Φx174 DNA (5,386 bp) incubated with the saturation concentration of 1,250 nM IHF in 200mM KCl. Compact DNA conformations were not observed.

In general, these AFM imaging results are consistent with the results from single-DNA stretching experiments: 1) DNA is more sharply bent in 100 mM and 50 mM KCl than in 200 mM KCl, and 2) in low salt concentration, the DNA bending angle non-monotonically depends on the concentration of IHF, as demonstrated in Figure 26D. In addition, we did not find apparent evidence that DNA can be condensed into higher order structures in 50 mM KCl. Such DNA condensation mechanism would predict DNA-protein complexes of varying sizes expected from inter-DNA aggregations mediated by IHF, while the sizes of the DNA-IHF complexes found in our AFM imaging experiments do not vary a lot.

3.6 IHF CONDENSES DNA INTO HIGHER ORDER STRUCTURES IN THE PRESENCE OF MAGNESIUM

Magnesium is essential for many enzymatic reactions in bacteria, and is present in bacteria at concentrations up to 4 mM [55]. It is also critical for chromosomal condensation and DNA repair [55, 56]. Recent experiments suggest that magnesium is also important for regulating the DNA binding properties of bacterial NAPs, such as H-NS and StpA [8, 36, 57]. This finding suggests that binding of IHF to DNA might be regulated by magnesium.

We used single-DNA stretching experiments to investigate the effects of magnesium on binding of IHF to DNA. To see the effects of magnesium on sharp DNA bending and DNA condensation, the KCl concentration was fixed at 50 mM. To minimize the

influence of DNA condensation on low force values, we first used the force jumping method to examine the effect of magnesium on DNA-IHF interactions. In the absence of magnesium, the force-extension curve shows a non-monotonic reduction of DNA extension (Fig. 22D and Fig. 28A). In the presence of IHF solution (250 nM and 1,250 nM) containing 2 mM $MgCl_2$, DNA condensation occurred at ~0.6 pN (Fig. 28A). Data points below 0.6 pN are not shown, because DNA extension was reduced to below 2 μm within 10 s at these force values and our magnetic tweezers setup could not measure extension below 2 μm (see Section 2.2.3 and Fig. 16B for details). The time courses during the force jumping experiments show the fast folding process that occurs at forces smaller than 0.6 pN before DNA extension was reduced below 2 μm (Fig. 28B-C). From these time courses, the speed at which DNA extension decreased exceeded 1 μm/s at ~0.3 pN. For comparison, folding in the absence of magnesium is much slower even at the lowest force of ~0.1 pN (Fig. 28D).

We used atomic force microscopy to confirm that magnesium enhanced DNA condensation mediated by IHF. In these experiments, DNA concentration was fixed at 0.2 ng/μl (converted to base pair molar concentration ~ 310 nM). At the 1,250 nM IHF and 50 mM KCl, the IHF-DNA complex was more compact in the presence of magnesium than without it (Fig. 26D & 29A). Different sizes of highly compact IHF-DNA complexes suggest that the different amounts of DNA are packaged inside each complex in Fig. 29A. Dilution of IHF concentrations to 310 nM (Fig. 29B) and 77.5 nM (Fig. 29C) reduces level of DNA compaction. At 31 nM IHF, DNA compaction is not observed (Fig. 29D). For comparison, in the presence of 200 mM KCl, where only the

weak DNA bending is allowed, single-DNA stretching experiment (Fig. 30A) and atomic force microscopy imaging (Fig. 30B-C) showed that magnesium does not influence the interaction of DNA and IHF.

These results indicate that magnesium promotes DNA compaction at low concentrations of KCl. Considering that IHF is an abundant NAP in all the growth phases of *E. coli* and magnesium exists *in vivo* in the mM range, these findings imply that the non-specific binding of IHF to bacterial DNA could be important for bacterial DNA compaction and organization of eDNA in biofilms.

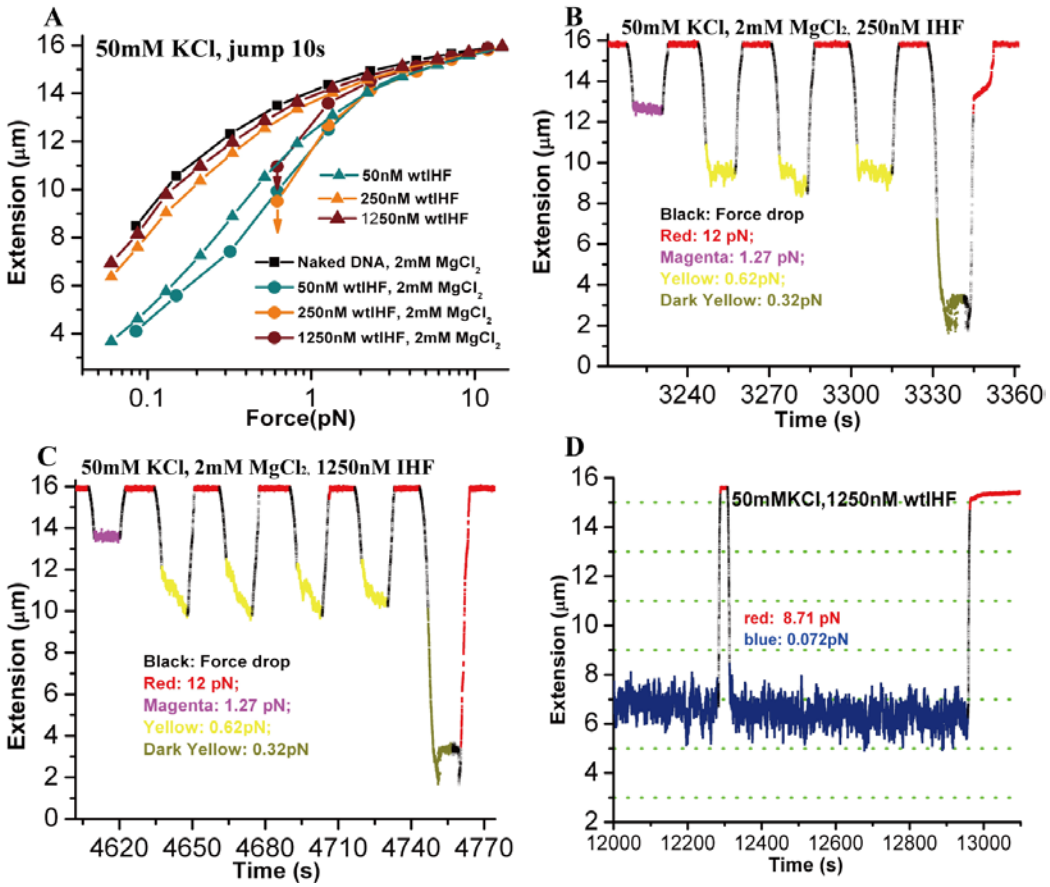

Figure 28. Effects of magnesium on DNA condensation in the presence of IHF by magnetic tweezers. **A)** Force-extension curves obtained using the quick force jumping method. Triangles and circles represent data obtained in the absence and presence of 2 mM $MgCl_2$, respectively. For 250 nM IHF and 1,250 nM IHF, data are not shown for force <0.6 pN because DNA extension was below the minimal extension (~2 μm) that could be measured by our instrument. **B-C)** DNA folding time course at various values of lower force and unfolding time course at the high force of ~12 pN in 250 nM IHF and 1,250 nM IHF, respectively. **D)** DNA folding time course of λ-DNA with 1250nM IHF in 50 mM KCl solution without magnesium. Folding in the absence of magnesium is much slower even at the lowest force of ~0.1 pN. The green dot grids are used as a comparison criterion for the DNA extension reduction.

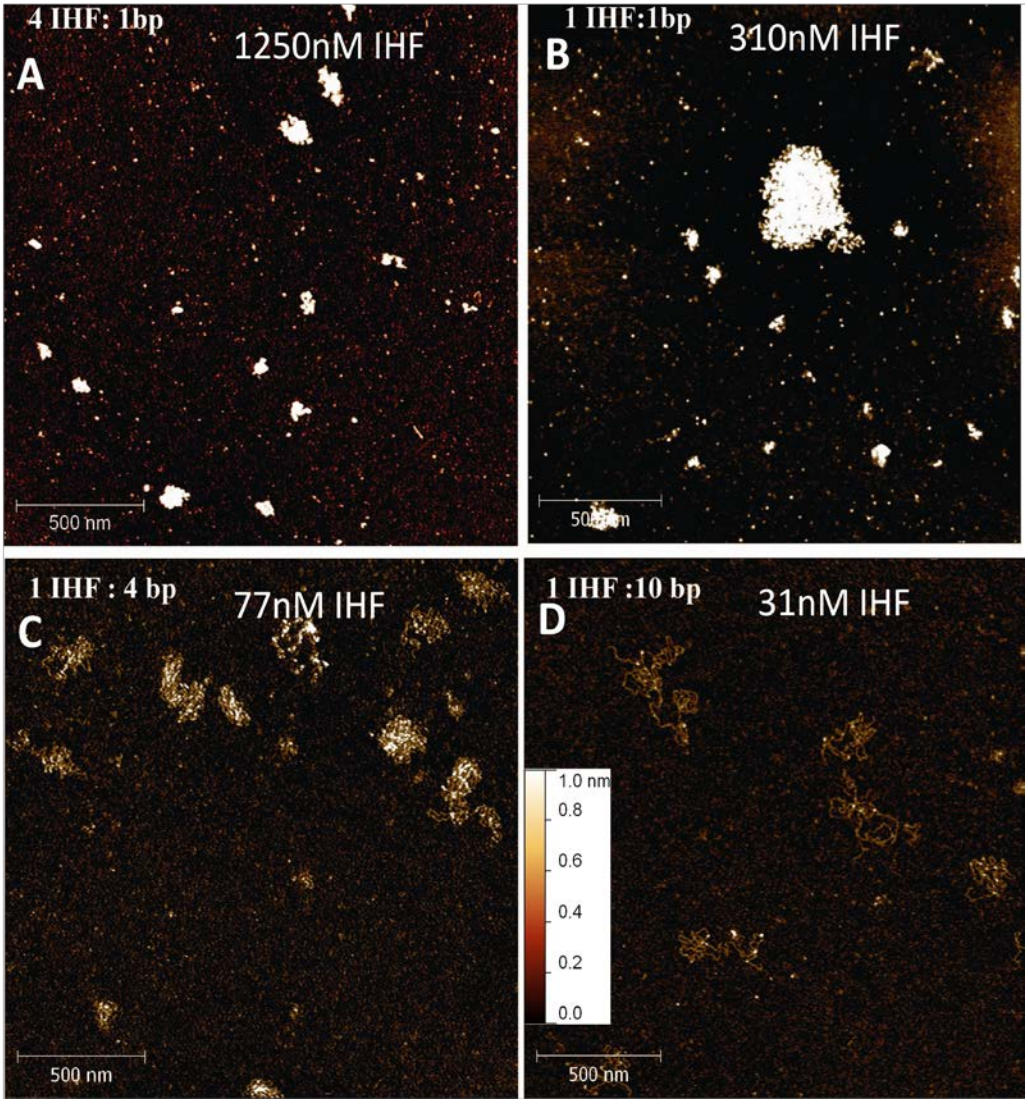

Figure 29. Atomic force microscopy analysis of effects of magnesium on linearized ΦX174 DNA (5,386 bp) condensation in the presence of IHF in 50 mM KCl, 2mM $MgCl_2$. **A)** DNA molecules incubated with 1,250 nM IHF (4 IHF: 1bp). **B)** DNA molecules incubated with 310 nM IHF (1 IHF: 1bp). **C)** DNA molecules incubated with 77 nM IHF (1 IHF: 4bp). **D)** DNA molecules incubated with 31 nM IHF (1 IHF: 10bp).

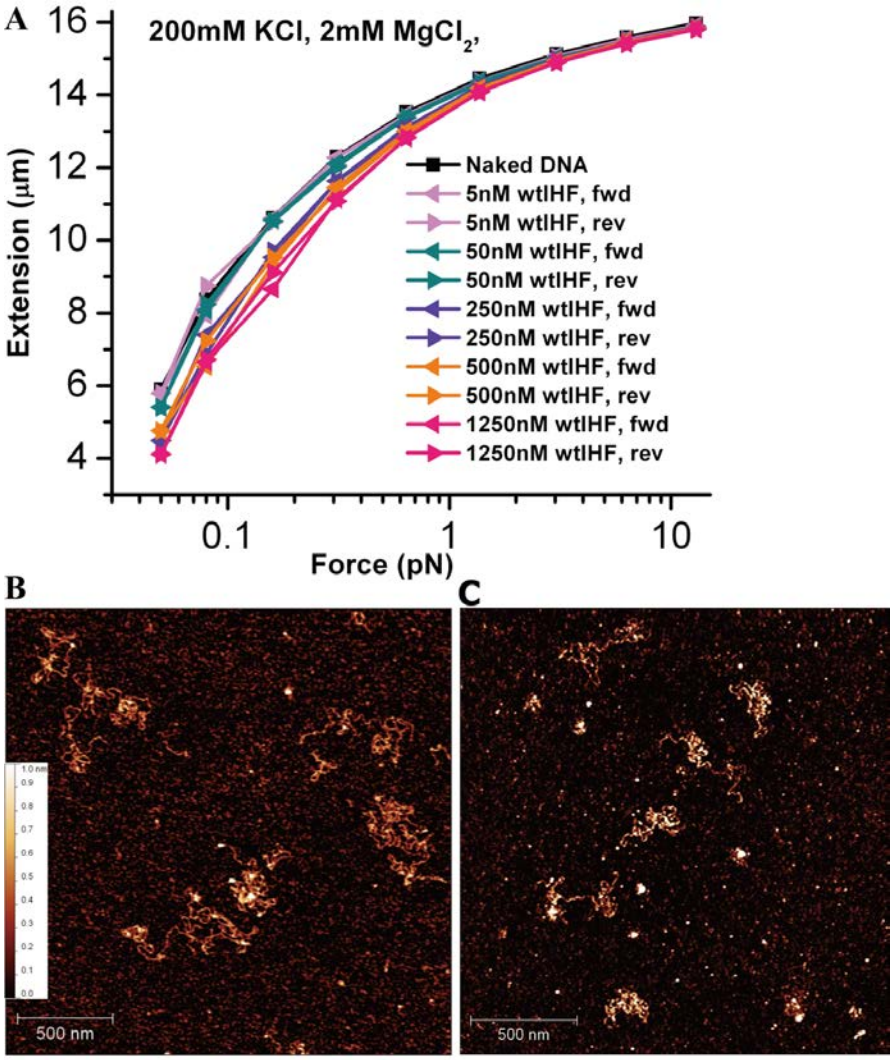

Figure 30. Magnesium does not have an apparent influence on DNA-IHF interaction in 200mM KCl, where only the weaker DNA bending occurs. **A)** Forward and reverse force-extension curves of λ-DNA at the indicated IHF concentrations in 200mMKCl solution. These curves are similar to those obtained in 200mM KCl in the absence of magnesium (Fig20A). **B-C)** AFM imaging of linearized Φx174 DNA (5,386 bp) molecules complexed with 1,250 nM IHF in 200 mM KCl in the absence of (B) and in the present of (C) 2 mM $MgCl_2$. These two images show great identities, which means that magnesium does not affect the conformation of DNA/IHF complex in 200 mM KCl.

CHAPTER 4: DISCUSSION AND CONCLUSION

4.1 SUMMARY OF DNA BINDING MODES OF IHF AND THEIR DEPENDENCE ON ENVIRONMENTAL FACTORS

Our results described in the last chapter indicate that the interaction between IHF and DNA is very complex, with IHF binding DNA through different modes that induce different DNA bending patterns. Furthermore, these different DNA binding modes are sensitive to environmental factors including KCl concentration, magnesium concentration, IHF concentration, and force. High concentrations of KCl induce weak DNA bending that is mediated by IHF. At high concentrations of KCl, a saturated concentration of IHF does not condense DNA further. At KCl concentration of 100 mM or less and unsaturated IHF concentration, a sharper DNA bending state appears.

This sharp bending state is inhibited at higher IHF concentrations, which leads to increased DNA extension as a function of the IHF concentration. This more extended DNA conformation is energetically favorable at high concentrations of IHF, because it will likely make more DNA available to accommodate more IHF proteins. Moreover, a physiological concentration of magnesium enhanced DNA compaction, suggesting a role of IHF in the packaging of bacterial DNA.

These DNA binding modes, their dependence on environmental factors, and the resulting DNA deformations and organizations are summarized and explained in Fig. 31

and its caption.

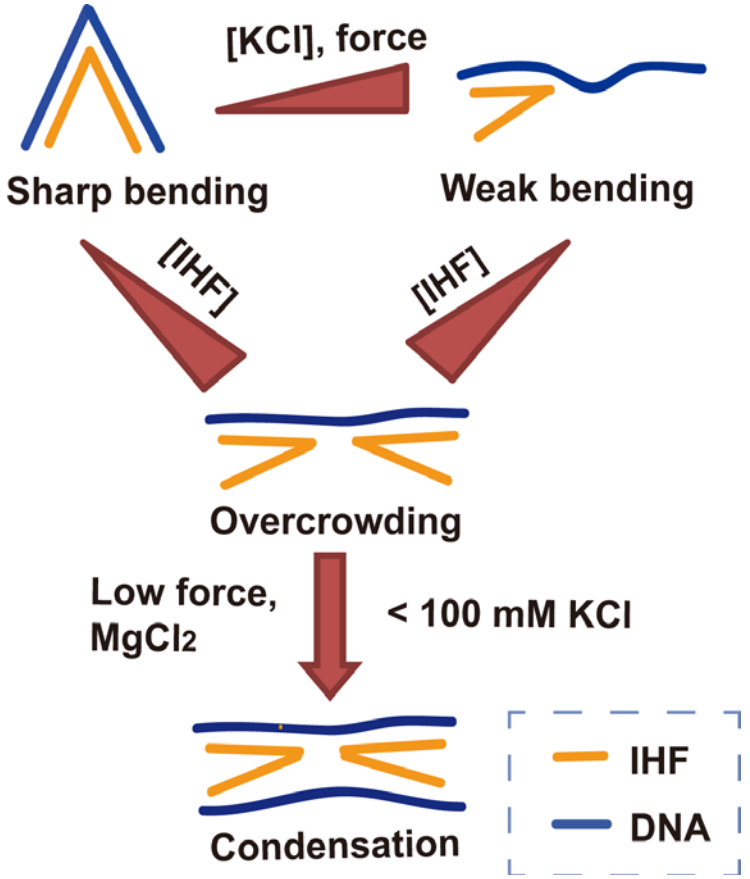

Figure 31. Schematic of the conformational states of the DNA-IHF complex and their dependence on force, [IHF], [KCl], and [$MgCl_2$]. Yellow represents an IHF dimer, and blue represents dsDNA. When binding of IHF is unsaturated, the weaker and sharper bending conformations are regulated by the concentration of KCl or tension. At high concentrations of IHF, DNA always adopts the weaker bending conformation regardless of the KCl concentration and tension due to overcrowding of IHF on DNA (middle). When overcrowding occurs at low concentrations of KCl, the exposed DNA interface that interacts with IHF can also interact with another DNA, leading to DNA condensation in the presence of magnesium.

4.2 IMPLICATIONS ON GLOBAL BACTERIAL GENE REGULATION

IHF influences global transcription in *E. coli* [16] and *S. typhimurium* [17]. It has been suggested that IHF positively regulates gene transcription by bending DNA to facilitate contact between regulatory proteins and RNA polymerase [19]. Our finding that IHF induces more than one DNA bending states that are mediated by several physiological factors suggests that gene regulation by IHF may be influenced by physiological factors that mediate DNA bending. However, regulation of specific genes by IHF is most likely controlled by high-affinity binding of IHF to specific DNA sequences, and the DNA conformations induced by these specific interactions may differ from those induced by non-specific interactions.

4.3 IMPLICATIONS ON PACKAGING OF CHROMOSOMAL DNA IN BACTERIA

IHF is the second most abundant NAP in the early stationery phase with a copy number of ~55,000 and a concentration of ~55μM [29]. Interestingly, the nucleoid of *E. coli* becomes more compact when it enters the stationary phase [6]. Because Dps is the most abundant NAP in the early stationery phase and it condenses DNA, Dps is believed to be responsible for the chromosomal DNA packaging in bacteria [58]. Our results suggest that IHF may also play a major role in DNA compaction during the early stationary phase, because it condenses DNA at physiological concentrations of magnesium. Additional studies are needed to determine how IHF contributes to DNA packaging in the presence of other NAPs.

4.4 IMPLICATIONS ON BIOFILM MAINTENANCE

In nature, bacteria form an organized, functional, and complex community called a biofilm. It has been estimated that most bacterial infections involve biofilm formation during the disease process [33]. Extracellular polymeric substances (EPS) that contain polysaccharides, proteins, nucleic acids, and lipids are critical to the formation and maintenance of biofilm [31]. The EPS provide the scaffold for the three-dimensional architecture of the biofilm and protect the bacteria within the biofilm [31].

Extracellular DNA (eDNA) is a common component of the EPS and forms a DNA meshwork. It has been shown that the eDNA meshwork plays an important role in stabilizing the biofilms [32]. Interestingly, IHF and Hu have been found in the eDNA meshwork [30, 33]. These proteins are critical for the integrity of the EPS matrix of biofilms, as removal of these proteins leads to biofilm disassembly or biofilm debulking [33]. Fluorescence imaging studies have shown that IHF and Hu localize to kinked DNA and crossed DNA within the eDNA meshwork of an NTHI biofilm [33]. These results support our finding that IHF can bend DNA and, in the presence of $MgCl_2$, condense DNA into a meshwork-like structure. Therefore, our results also provide insights into the structural roles of IHF in supporting biofilm integrity.

4.5 RELEVANCE OF BENDING INDUCED BY SPECIFIC AND NON-SPECIFIC IHF BINDING

Binding of IHF to the 34-bp H' sequence induces a sharp DNA bend that exceeds ~160^{o}. To determine if the sharper DNA bending caused by non-specific binding of IHF is similar to the bending the H' sequence by IHF, we simulated the reduction of DNA extension at 0.1 pN as a function of bending angle and the density of IHF bound to DNA using the worm-like-chain polymer model of DNA.

According to experiments, at 0.1 pN, the extension of DNA decreased the most at IHF concentrations of 250 nM in 100 mM KCL and 50 nM in 50 nM KCl, where DNA extension was shortened by ~50% (see Fig. 22E). To compare with the experiments, we simulated the values of the density of IHF and the bending angles that can decrease extension by 50% at 0.1 pN (Fig. 32). For a bending angle of 160^{o}, low protein occupancy around one IHF per 400 bp would be required to reduce extension by 50%. However, in our experiments, the greatest decrease in extension occurred at critical concentrations of IHF above which overcrowding of IHF occurs. Therefore, we expect that the IHF occupancy should be much higher when extension is decreased maximally. This finding suggests that in the non-specific DNA binding mode, DNA in the sharper bending state in 100 mM KCl and 50 mM KCl is still much less bent than H' bent by IHF in the specific binding.

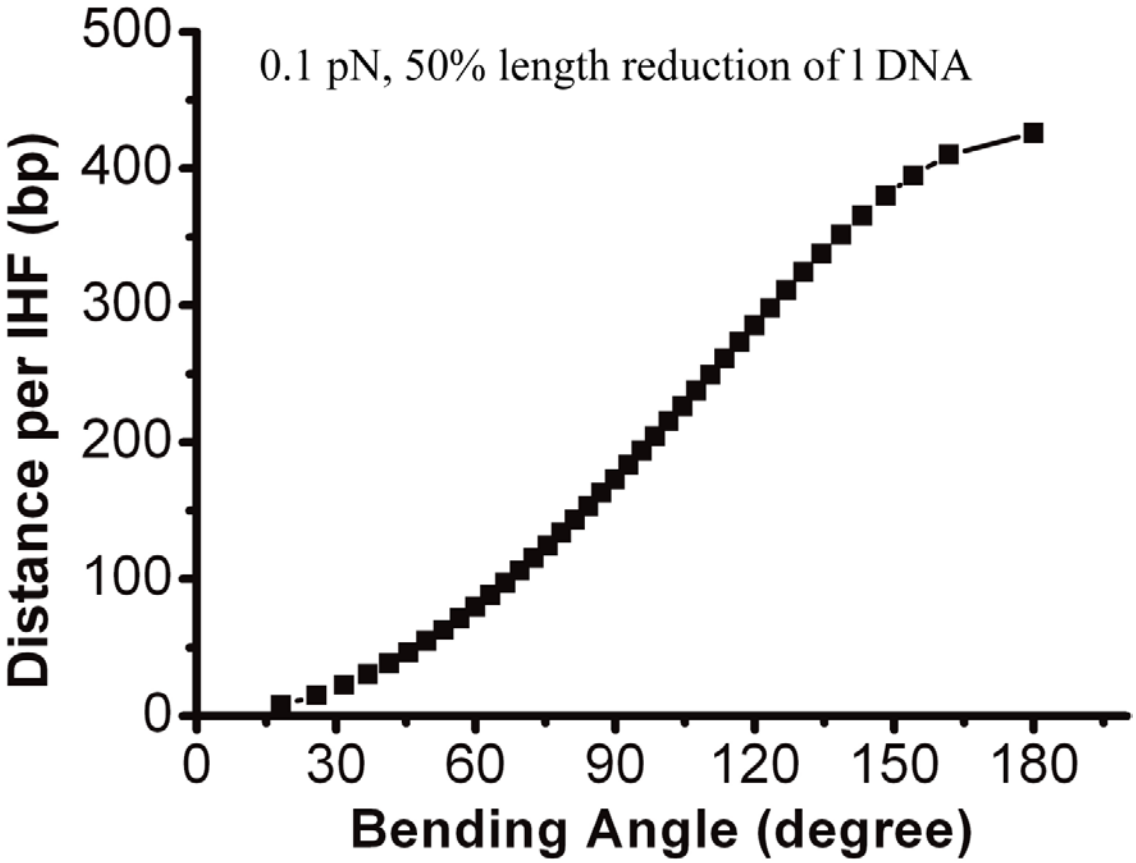

Figure 32. The occupancy of IHF bound to DNA predicted to introduce a DNA bending angle that causes 50% reduction in DNA extension at 0.1 pN as a function of DNA bending angle.

4.6 CONCLUSION

In summary, we show that distinct modes of non-specific binding of IHF to DNA result in complex DNA conformations. Changes in KCl concentration, IHF concentration, and force can change the sharpness of DNA bending. In addition, IHF can crosslink DNA into a highly compact meshwork structure that is enhanced by magnesium. Our findings

provide insights into the interactions and functions of IHF in bacterial gene regulation, chromosome packaging, and biofilm maintenance.

REFERENCE

1. KUBITSCHEK, H.E., *CELL VOLUME INCREASE IN ESCHERICHIA COLI AFTER SHIFTS TO RICHER MEDIA.* J. BACTERIOL., 1990. 172(1): P. 94-101.

2. CHO, B.-K. AND B.Ø. PALSSON, *CAN THE PROTEIN OCCUPANCY LANDSCAPE SHOW THE TOPOLOGICALLY ISOLATED CHROMOSOMAL DOMAINS IN THE E. COLI GENOME?: AN EXCITING PROSPECT.* MOLECULAR CELL, 2009. 35(3): P. 255-256.

3. BROWNING, D.F., D.C. GRAINGER, AND S.J. BUSBY, *EFFECTS OF NUCLEOID-ASSOCIATED PROTEINS ON BACTERIAL CHROMOSOME STRUCTURE AND GENE EXPRESSION.* CURR OPIN MICROBIOL, 2010. 13(6): P. 773-80.

4. ALI AZAM, T., ET AL., *GROWTH PHASE-DEPENDENT VARIATION IN PROTEIN COMPOSITION OF THE ESCHERICHIA COLI NUCLEOID.* J BACTERIOL, 1999. 181(20): P. 6361-70.

5. SINGER, B.S., ET AL., *LIBRARIES FOR GENOMIC SELEX.* NUCLEIC ACIDS RES, 1997. 25(4): P. 781-6.

6. FRENKIEL-KRISPIN, D., ET AL., *REGULATED PHASE TRANSITIONS OF BACTERIAL CHROMATIN: A NON-ENZYMATIC PATHWAY FOR GENERIC DNA PROTECTION.* EMBO J, 2001. 20(5): P. 1184-91.

7. MAURER, S., J. FRITZ, AND G. MUSKHELISHVILI, *A SYSTEMATIC IN VITRO STUDY OF NUCLEOPROTEIN COMPLEXES FORMED BY BACTERIAL NUCLEOID-ASSOCIATED PROTEINS REVEALING NOVEL TYPES OF DNA ORGANIZATION.* J MOL BIOL, 2009. 387(5): P. 1261-76.

8. LIU, Y., ET AL., *A DIVALENT SWITCH DRIVES H-NS/DNA-BINDING CONFORMATIONS BETWEEN STIFFENING AND BRIDGING MODES.* GENES DEV, 2010. 24(4): P. 339-44.

9. DILLON, S.C. AND C.J. DORMAN, *BACTERIAL NUCLEOID-ASSOCIATED PROTEINS, NUCLEOID STRUCTURE AND GENE EXPRESSION.* NAT REV MICROBIOL, 2010. 8(3): P. 185-95.

10. MCLEOD, S.M., ET AL., *THE C-TERMINAL DOMAINS OF THE RNA POLYMERASE ALPHA SUBUNITS: CONTACT SITE WITH FIS AND LOCALIZATION DURING CO-ACTIVATION WITH CRP AT THE ESCHERICHIA COLI PROP P2 PROMOTER.* J MOL BIOL, 2002. 316(3): P. 517-29.

11. GRAINGER, D.C., ET AL., *ASSOCIATION OF NUCLEOID PROTEINS WITH CODING AND NON-CODING SEGMENTS OF THE ESCHERICHIA COLI GENOME.* NUCLEIC ACIDS RES, 2006. 34(16): P. 4642-52.

12. WIGGINS, P.A., ET AL., *PROTEIN-MEDIATED MOLECULAR BRIDGING: A KEY MECHANISM IN BIOPOLYMER ORGANIZATION.* BIOPHYS J, 2009. 97(7): P. 1997-2003.

13. ISHIHAMA, A., *PROKARYOTIC GENOME REGULATION: MULTIFACTOR PROMOTERS, MULTITARGET REGULATORS AND HIERARCHIC NETWORKS.* FEMS MICROBIOL REV, 2010. 34(5): P. 628-45.

14. NASH, H.A. AND C.A. ROBERTSON, *PURIFICATION AND PROPERTIES OF THE ESCHERICHIA COLI PROTEIN FACTOR REQUIRED FOR LAMBDA INTEGRATIVE RECOMBINATION.* J BIOL CHEM, 1981. 256(17): P. 9246-53.

15. RICE, P.A., ET AL., *CRYSTAL STRUCTURE OF AN IHF-DNA COMPLEX: A PROTEIN-INDUCED DNA U-TURN.* CELL, 1996. 87(7): P. 1295-306.

16. ARFIN, S.M., ET AL., *GLOBAL GENE EXPRESSION PROFILING IN ESCHERICHIA COLI K12. THE EFFECTS OF INTEGRATION HOST FACTOR.* J BIOL CHEM, 2000. 275(38): P. 29672-84.

17. MANGAN, M.W., ET AL., *THE INTEGRATION HOST FACTOR (IHF) INTEGRATES STATIONARY-PHASE AND VIRULENCE GENE EXPRESSION IN SALMONELLA ENTERICA SEROVAR TYPHIMURIUM.* MOLECULAR MICROBIOLOGY, 2006. 59(6): P. 1831-47.

18. CASES, I. AND V. DE LORENZO, *PROMOTERS IN THE ENVIRONMENT: TRANSCRIPTIONAL REGULATION IN ITS NATURAL CONTEXT.* NAT REV MICROBIOL, 2005. 3(2): P. 105-18.

19. SANTERO, E., ET AL., *ROLE OF INTEGRATION HOST FACTOR IN STIMULATING TRANSCRIPTION FROM THE SIGMA 54-DEPENDENT NIFH PROMOTER.* J MOL BIOL, 1992. 227(3): P. 602-20.

20. GOODRICH, J.A., M.L. SCHWARTZ, AND W.R. MCCLURE, *SEARCHING FOR AND PREDICTING THE ACTIVITY OF SITES FOR DNA BINDING PROTEINS: COMPILATION AND ANALYSIS OF THE BINDING SITES FOR ESCHERICHIA COLI INTEGRATION HOST FACTOR (IHF).* NUCLEIC ACIDS RES, 1990. 18(17): P. 4993-5000.

21. ENGELHORN, M., ET AL., *IN VIVO INTERACTION OF THE ESCHERICHIA COLI INTEGRATION HOST FACTOR WITH ITS SPECIFIC BINDING SITES.* NUCLEIC ACIDS RES, 1995. 23(17): P. 2959-65.

22. USSERY, D., ET AL., *GENOME ORGANISATION AND CHROMATIN STRUCTURE IN ESCHERICHIA COLI.* BIOCHIMIE, 2001. 83(2): P. 201-12.

23. WANG, S., ET AL., *THE SPECIFIC BINDING OF ESCHERICHIA COLI INTEGRATION HOST FACTOR INVOLVES BOTH MAJOR AND MINOR GROOVES OF DNA.* BIOCHEMISTRY, 1995. 34(40): P. 13082-90.

24. YANG, S.W. AND H.A. NASH, *COMPARISON OF PROTEIN BINDING TO DNA IN VIVO AND IN VITRO: DEFINING AN EFFECTIVE INTRACELLULAR TARGET.* EMBO J, 1995. 14(24): P. 6292-300.

25. MURTIN, C., ET AL., *A QUANTITATIVE UV LASER FOOTPRINTING ANALYSIS OF THE INTERACTION OF IHF WITH SPECIFIC BINDING SITES: RE-EVALUATION OF THE EFFECTIVE CONCENTRATION OF IHF IN THE CELL.* J MOL BIOL, 1998. 284(4): P. 949-61.

26. CRAIG, N.L. AND H.A. NASH, *E. COLI INTEGRATION HOST FACTOR BINDS TO SPECIFIC SITES IN DNA.* CELL, 1984. 39(3 PT 2): P. 707-16.

27. NIENHUIS, A.W., ET AL., *EXPRESSION OF THE HUMAN C-FMS PROTO-ONCOGENE IN HEMATOPOIETIC CELLS AND ITS DELETION IN THE 5Q- SYNDROME.* CELL, 1985. 42(2): P. 421-8.

28. SUGIMURA, S. AND D.M. CROTHERS, *STEPWISE BINDING AND BENDING OF DNA BY ESCHERICHIA COLI INTEGRATION HOST FACTOR.* PROC NATL ACAD SCI U S A, 2006. 103(49): P. 18510-4.

29. DITTO, M.D., D. ROBERTS, AND R.A. WEISBERG, *GROWTH PHASE VARIATION OF INTEGRATION HOST FACTOR LEVEL IN ESCHERICHIA COLI.* J BACTERIOL, 1994. 176(12): P. 3738-48.

30. STINSON, M.W. AND E.J. BERGEY, *ISOLATION OF HEART- AND KIDNEY-BINDING PROTEIN FROM GROUP A STREPTOCOCCI.* INFECT IMMUN, 1982. 35(1): P. 335-42.

31. FLEMMING, H.C. AND J. WINGENDER, *THE BIOFILM MATRIX.* NAT REV MICROBIOL, 2010. 8(9): P. 623-33.

32. WHITCHURCH, C.B., ET AL., *EXTRACELLULAR DNA REQUIRED FOR BACTERIAL BIOFILM FORMATION.* SCIENCE, 2002. 295(5559): P. 1487.

33. GOODMAN, S.D., ET AL., *BIOFILMS CAN BE DISPERSED BY FOCUSING THE IMMUNE SYSTEM ON A COMMON FAMILY OF BACTERIAL NUCLEOID-ASSOCIATED PROTEINS.* MUCOSAL IMMUNOL, 2011. 4(6): P. 625-37.

34. YAN, J. AND J.F. MARKO, *EFFECTS OF DNA-DISTORTING PROTEINS ON DNA ELASTIC RESPONSE.* PHYS REV E STAT NONLIN SOFT MATTER PHYS, 2003. 68(1 PT 1): P. 011905.

35. YAN, J., R. KAWAMURA, AND J.F. MARKO, *STATISTICS OF LOOP FORMATION ALONG DOUBLE HELIX DNAS.* PHYS REV E STAT NONLIN SOFT MATTER PHYS, 2005. 71(6 PT 1): P. 061905.

36. LIM, C.J., ET AL., *GENE SILENCING H-NS PARALOGUE STPA FORMS A RIGID PROTEIN FILAMENT ALONG DNA THAT BLOCKS DNA ACCESSIBILITY.* NUCLEIC ACIDS RESEARCH, 2011.

37. WATSON, J.D. AND F.H. CRICK, *MOLECULAR STRUCTURE OF NUCLEIC ACIDS; A STRUCTURE FOR DEOXYRIBOSE NUCLEIC ACID.* NATURE, 1953. 171(4356): P. 737-8.

38. SMITH, S.B., L. FINZI, AND C. BUSTAMANTE, *DIRECT MECHANICAL MEASUREMENTS OF THE ELASTICITY OF SINGLE DNA MOLECULES BY USING MAGNETIC BEADS.* SCIENCE, 1992. 258(5085): P. 1122-6.

39. BUSTAMANTE, C., ET AL., *ENTROPIC ELASTICITY OF LAMBDA-PHAGE DNA.* SCIENCE, 1994. 265(5178): P. 1599-600.

40. SIGGIA, J.F.M.E.D., *STRETCHING DNA.* MACROMOLECULES 1995. 28(26): P. 8759-8770.

41. COCCO, S., ET AL., *OVERSTRETCHING AND FORCE-DRIVEN STRAND SEPARATION OF DOUBLE-HELIX DNA.* PHYS REV E STAT NONLIN SOFT MATTER PHYS, 2004. 70(1 PT 1): P. 011910.

42. NEUMAN, K.C. AND A. NAGY, *SINGLE-MOLECULE FORCE SPECTROSCOPY: OPTICAL TWEEZERS, MAGNETIC TWEEZERS AND ATOMIC FORCE MICROSCOPY.* NAT METHODS, 2008. 5(6): P. 491-505.

43. JAMES E. KATH, J.F.M., JOHN S. GRAHAM, *DEVELOPMENT OF A MAGNETIC TWEEZER APPARATUS FOR THE MANIPULATION OF SINGLE DNA MOLECULES.* NANOSCAPE, 2008. 5(1): P. 117-123.

44. CHEN, H., ET AL., *IMPROVED HIGH-FORCE MAGNETIC TWEEZERS FOR STRETCHING AND REFOLDING OF PROTEINS AND SHORT DNA.* BIOPHYS J, 2011. 100(2): P. 517-23.

45. YAN, J., D. SKOKO, AND J.F. MARKO, *NEAR-FIELD-MAGNETIC-TWEEZER MANIPULATION OF SINGLE DNA MOLECULES.* PHYS REV E STAT NONLIN SOFT MATTER PHYS, 2004. 70(1 PT 1): P. 011905.

46. LIU, Y., ET AL., *DNA CONDENSATES ORGANIZED BY THE CAPSID PROTEIN VP15 IN WHITE SPOT SYNDROME VIRUS.* VIROLOGY, 2010. 408(2): P. 197-203.

47. HANSMA, D.R.P., *ATOMIC FORCE MICROSCOPY* PHYSICS TODAY, 1990. 43(10): P. 23-30.

48. KE, C., ET AL., *DIRECT MEASUREMENTS OF BASE STACKING INTERACTIONS IN DNA BY SINGLE-MOLECULE ATOMIC-FORCE SPECTROSCOPY.* PHYS REV LETT, 2007. 99(1): P. 018302.

49. CHEN, W.S., ET AL., *DIRECT OBSERVATION OF MULTIPLE PATHWAYS OF SINGLE-STRANDED DNA STRETCHING.* PHYS REV LETT, 2010. 105(21): P. 218104.

50. HANSMA, H.G. AND D.E. LANEY, *DNA BINDING TO MICA CORRELATES WITH CATIONIC RADIUS: ASSAY BY ATOMIC FORCE MICROSCOPY.* BIOPHYS J, 1996. 70(4): P. 1933-9.

51. WANG, H., ET AL., *GLUTARALDEHYDE MODIFIED MICA: A NEW SURFACE FOR ATOMIC FORCE MICROSCOPY OF CHROMATIN.* BIOPHYS J, 2002. 83(6): P. 3619-25.

52. FU, H., ET AL., *ATOMIC FORCE MICROSCOPE IMAGING OF CHROMATIN ASSEMBLED IN XENOPUS LAEVIS EGG EXTRACT.* CHROMOSOMA, 2011. 120(3): P. 245-54.

53. BAO, Q., N. CHRIST, AND P. DROGE, *SINGLE-CHAIN INTEGRATION HOST FACTORS AS PROBES FOR HIGH-PRECISION NUCLEOPROTEIN COMPLEX FORMATION.* GENE, 2004. 343(1): P. 99-106.

54. ALI, B.M., ET AL., *COMPACTION OF SINGLE DNA MOLECULES INDUCED BY BINDING OF INTEGRATION HOST FACTOR (IHF).* PROC NATL ACAD SCI U S A, 2001. 98(19): P. 10658-63.

55. LUSK, J.E., R.J.P. WILLIAMS, AND E.P. KENNEDY, *MAGNESIUM AND GROWTH OF ESCHERICHIA COLI.* JOURNAL OF BIOLOGICAL CHEMISTRY, 1968. 243(10): P. 2618-+.

56. PAYMASTER, N.J., *MAGNESIUM-METABOLISM - BRIEF REVIEW.* ANNALS OF THE ROYAL COLLEGE OF SURGEONS OF ENGLAND, 1976. 58(4): P. 309-314.

57. WALTHERS, D., ET AL., *SALMONELLA ENTERICA RESPONSE REGULATOR SSRB RELIEVES H-NS SILENCING BY DISPLACING H-NS BOUND IN POLYMERIZATION MODE AND DIRECTLY ACTIVATES TRANSCRIPTION.* JOURNAL OF BIOLOGICAL CHEMISTRY, 2011. 286(3): P. 1895-1902.

58. AZAM, T.A., S. HIRAGA, AND A. ISHIHAMA, *TWO TYPES OF LOCALIZATION OF THE DNA-BINDING PROTEINS WITHIN THE ESCHERICHIA COLI NUCLEOID.* GENES CELLS, 2000. 5(8): P. 613-26.